Absolute optical oscillator strengths for the electronic excitation of atoms at high resolution. III. The photoabsorption of argon, krypton, and xenon

W. F. Chan, G. Cooper, X. Guo,* G. R. Burton, and C. E. Brion
Department of Chemistry, The University of British Columbia, 2036 Main Mall, Vancouver, British Columbia, Canada V6T 1Z1
(Received 23 December 1991)

Absolute oscillator strengths for the photoabsorption of argon, krypton, and xenon in both the discrete and continuum regions have been measured. The results are compared where possible with previously published experimental and theoretical data. The present work is a continuation of recently reported measurements for helium [Chan *et al.*, Phys. Rev. A **44**, 186 (1991)] and neon [Chan *et al.*, Phys. Rev. A **45**, 1420 (1992)] obtained using the dipole (e,e) method at both low and high resolution. Using the low-resolution dipole (e,e) spectrometer [with a full width at half maximum (FWHM) of about 1 eV], absolute photoabsorption oscillator strength spectra for the valence and inner shells of argon, krypton, and xenon were obtained up to equivalent photon energies of 500, 380, and 398 eV, respectively. The high-resolution dipole (e,e) spectrometer (FWHM of 0.048 eV) was employed to obtain absolute photoabsorption oscillator strengths for the discrete electronic transitions from the ground states to the ms^2mp^5ns and ms^2mp^5nd $(^2P_{3/2,1/2})$ manifolds where $m=3$, 4, and 5 for argon, krypton, and xenon, respectively. The absolute optical oscillator strength scales were obtained by single-point continuum normalization of the Bethe-Born converted electron-energy-loss spectra using the recently reported absolute optical data of Samson and Yin [J. Opt. Soc. Am. B **6**, 2326 (1989)] for argon, krypton, and xenon atoms. High-resolution absolute photoabsorption oscillator strengths were also obtained in the energy regions of the autoionizing resonances corresponding to excitation of the inner-valence s electrons of argon, krypton, and xenon.

PACS number(s): 32.70.Cs, 32.30.Dx, 32.80.Fb

I. INTRODUCTION

Absolute optical oscillator strengths for atoms and molecules in the discrete and continuum regions provide valuable quantitative information for further understanding the electronic structure of matter and its interaction with energetic electromagnetic radiation. This information is of importance in areas of application such as radiation-induced decomposition, plasma physics, astronomy, biophysics, and the testing and development of theoretical methods. Similar to the situation for neon [1–8], the photoionization cross-section maxima of argon and krypton [2–9] are shifted to energies above the ionization threshold, showing significant departure from the hydrogenic model. While this departure is not so obvious for xenon [3,4,6–8] it does nevertheless show significant nonhydrogenic behavior. In addition, minima (sometimes called the Cooper minima) have been observed in the photoionization cross sections of argon, as well as krypton and xenon [1–10]. Instead of using a pure Coulomb nuclear potential, Cooper [1], employing a more realistic potential similar to the Hartree-Fock potential for the outer subshell of each atom, and also both Manson and Cooper [10] and McGuire [2], starting with Herman-Skillman central potentials, have been able to theoretically reproduce the maxima above the threshold and also the existence of the minima in the photoionization cross sections starting from one-electron approximations. However, the above calculations give narrower peaks shifted in energy relative to the experimental cross sections, with the cross sections at the peak maxima two or three times higher than the experimental values. The $4d$ shell in xenon is an example where significant discrepancies between experimental and theoretical results have been observed. It has been found that electron correlation is important in many cases [3–9,11]. With the inclusion of electron correlation, the calculated photoionization cross sections [3,5–8] are generally in better agreement with experiment; however, some discrepancies ($>20\%$) still remain between the experimental and theoretical values in certain energy ranges.

Experimentally, photoabsorption and photoionization cross-section measurements in the ionization continuum regions of argon, krypton, and xenon have been widely performed using Beer-Lambert law photoabsorption and the double-ion-chamber methods [12–29]. Line-emitting light sources [12,14–17,19,21,28,29] have most commonly been used. The Hopfield continuum [13,18], generated by a repetitive, condensed discharge through helium, provides a useful continuum source in the energy region 11.3–21.4 eV. With the advance of synchrotron radiation an intense and continuous light source has become available for measuring the photoionization cross sections of atoms and molecules up to high energies [20,22–27]. However, contributions from stray light and higher-order radiation have to be carefully assessed and the measurements appropriately corrected if synchrotron radiation is to be used as the light source for accurate absolute cross-section measurements [30–32]. These Beer-Lambert photoionization measurements give good agreement for the individual noble gases in terms of the shapes of the continua. However, the absolute values of the pho-

toabsorption cross sections in the continuum typically show substantial differences ($\sim 10\%$), especially at higher energies, due to difficulties in obtaining precise measurements of the sample target density in a "windowless" far-UV system and also due to contributions from stray light and/or higher-order radiation. By using the dipole excitation associated with inelastic scattering of electron beams of high impact energy (10 keV) and small scattering angle, the single and multiple photoionization of argon [33], krypton, and xenon [34] has been studied using electron-ion coincidence techniques. Relative optical oscillator strengths were obtained [33,34] by Bethe-Born conversion of electron-scattering data and absolute scales were established by normalizing at single energies to previously published [19] absolute photoabsorption cross sections.

For the excitation of the heavier noble-gas atoms in the discrete region, several theoretical oscillator strength calculations have been reported. Cooper [1], employing a one-electron central potential model, and Amus'ya [35], applying the random-phase approximation with exchange (RPAE) method, have calculated the oscillator strengths for the transitions from the ground states to the $ms^2mp^5(^2P_{3/2,1/2})ns$ and nd states where $n > m$ and m is 3, 4, and 5 for argon, krypton, and xenon, respectively. Calculations of the oscillator strengths for the separate transitions from the ground states to the $ms^2mp^5(^2P_{3/2})ns$ and nd states, and the $ms^2mp^5(^2P_{1/2})ns'$ and nd' states have also been reported [36–47], but mostly these calculations only give oscillator strengths for the $ms^2mp^5(^2P_{3/2})(m+1)s$ and $ms^2mp^5(^2P_{1/2})(m+1)s'$ states [36–40,43–47].

Because the valence-shell electronic transitions of noble-gas atoms have extremely narrow natural linewidths, absolute oscillator strength measurements for the discrete regions of the argon, krypton, and xenon photoabsorption spectra via the Beer-Lambert law are questionable since significant errors may arise due to so-called "line-saturation" (i.e., bandwidth) effects. Detailed discussions of line-saturation effects and their implications for absolute photoabsorption oscillator strength (cross section) measurements have been given in Refs. [48–51]. Several alternative experimental methods for determining discrete optical oscillator strengths which avoid line-saturation problems have been reported. However, in most cases these methods are somewhat complex and also are often severely restricted in their range of application so that only a very few transitions can be studied for a given target [49]. In the cases of argon, krypton, and xenon, other techniques that have been used include the self-absorption method [52–55], the total (optical) absorption method [56–58], the linear absorption method [59], refraction index determination [60], lifetime measurements [61–68], pressure-broadening profile analysis [69–73], phase-matching techniques [74,75], study of the electron excitation function [76], and electron-impact methods [77–86]. The electron-impact-based methods which have been employed for measuring the discrete optical oscillator strengths of argon, krypton, and xenon can be summarized as follows. By using very high impact energy (25–32 keV) and very small scattering angle ($\sim 1\times 10^{-4}$ rad), Geiger [77,79,80,82,83] obtained optical oscillator strengths for the resonance lines of the noble gases by converting the electron-energy-loss spectra to relative optical spectra and normalizing on the elastic differential cross section. In other electron-impact work Li *et al.* [84] for argon, Takayanagi *et al.* [85] for krypton, and Delage and Carette [81] and also Suzuki *et al.* [86] for xenon have reported optical oscillator strengths for resonance lines in the heavier noble gases by extrapolating the generalized oscillator strengths of lines, measured at different scattering angles and at low electron-impact energy, to zero momentum transfer. Delage and Carette [81] normalized their data on one of the transition peaks of xenon that was measured by Geiger [80], while Li *et al.* [84], Takayanagi *et al.* [85], and Suzuki *et al.* [86] normalized their data on the elastic-scattering cross section. The unpublished electron impact work of Natali, Kuyatt, and Miekzarek [87] for the optical oscillator strengths of the noble gases has been quoted in references [53,82,88].

Consideration of the various experimental and theoretical oscillator strength values published to date for argon, krypton, and xenon shows that there is a large body of existing information for the continuum regions. In contrast there is relatively little information available in the valence-shell discrete region. For the *discrete* spectra of argon, krypton, and xenon only the transitions to the $ms^2mp^5(^2P_{3/2})(m+1)s$ and $ms^2mp^5(^2P_{1/2})(m+1)s'$ states, where m is 3, 4, and 5, respectively, have been studied in any detail and even for these considerable variations in oscillator strength values have been reported. In the case of argon the optical oscillator strength data available in 1975 was reviewed by Eggarter [89] for both the discrete and continuum regions up to 3202 eV. On the basis of the information available Eggarter [89] listed recommended optical oscillator strength values for argon.

In part I [49] and part II [90] of this series of studies on the photoabsorption of the noble gases, we have reported detailed and comprehensive measurements for helium [49] and neon [90]. These results were obtained using a recently developed highly accurate high-resolution electron-impact-based method for obtaining absolute optical oscillator strengths for the discrete, continuum, and autoionizing resonance regions in atoms and molecules. This method [49,90] is not subject to the line-saturation effects which can cause serious errors in Beer-Lambert law photoabsorption experiments when the bandwidth is comparable to or larger than the natural linewidth. The method involves combining measurements obtained using a high-resolution (HR) [0.048 eV full width at half maximum (FWHM)] dipole (e,e) spectrometer in conjunction with a lower-resolution (~ 1 eV FWHM) dipole (e,e) instrument. All measurements are made at high impact energies and zero-degree scattering angle (i.e., negligible momentum transfer) corresponding to the "optical limit" so that no extrapolation procedures are required. The absolute oscillator strength scales for helium and neon were obtained by Thomas-Reiche-Kuhn (TRK) sum-rule normalization and were thus completely independent of any direct optical measurement. The same general method is now applied to provide independent and wide-

ranging measurements of the absolute photoabsorption oscillator strengths for the discrete, continuum, and autoionizing resonance regions of argon, krypton, and xenon. However, in practice the valence-shell TRK sum-rule normalization procedures which were employed for helium [49] and neon [90] are difficult to apply for the heavier noble gases due to difficulties in carrying out the necessary lengthy valence-shell extrapolations. These difficulties arise because of the smaller energy separations between the different subshells of the argon, krypton, and xenon atoms compared with the relatively simple electronic configurations of helium and neon. The absolute scales of the presently reported data have therefore been obtained by normalizing on recently reported high precision valence-shell photoabsorption oscillator strengths measured at helium and neon resonance line photon energies by Samson and Yin [28]. In the present work we now report measurements of (i) absolute total photoabsorption oscillator strengths for argon, krypton, and xenon up to 500, 380, and 398 eV, respectively, at a resolution of 1 eV FWHM, (ii) absolute photoabsorption oscillator strengths for the discrete dipole-allowed electronic transitions from the mp^6 subshells to levels of the lower members of the ms^2mp^5ns and ms^2mp^5nd ($^2P_{3/2,1/2}$) manifolds where $n > m$ and m is 3, 4, and 5 for argon, krypton, and xenon, respectively, at a resolution of 0.048 eV FWHM, and (iii) absolute photoabsorption oscillator strengths in the regions of the Beutler-Fano autoionization resonance profiles involving excitation of the inner-valence ms electrons at a resolution of 0.048 eV FWHM. These results are compared with previously published experimental and theoretical data in regions where such data are available.

II. EXPERIMENTAL METHOD

The experimental procedures used in the present work are similar to those employed earlier for the measurements on helium [49] and neon [90]. Briefly, a low-resolution ($\sim$1 eV FWHM) dipole (e,e) spectrometer with high impact energy (8 keV) and zero-degree ($\theta=0°$) scattering angle (acceptance angle of 1.4×10^{-4} sr) was employed to obtain electron-energy-loss measurements for argon, krypton, and xenon in the energy ranges 10–500, 8–380, and 7–398 eV, respectively. Relative optical oscillator strengths were obtained by transforming the electron-energy-loss data using the known Bethe-Born conversion factor of the spectrometer. The TRK valence-shell sum-rule normalization procedure used to establish the absolute scales for helium and neon could not be used for the heavier noble gases since the successive atomic inner-subshell energy separations are relatively small. In these circumstances the extrapolation procedures used to estimate the amount of valence-shell oscillator strength above a certain energy become unreliable for argon, krypton, and xenon. Therefore the alternative procedure of single-point normalization to a photoabsorption measurement has been used. Recently Samson and Yin [28] have reported very precise measurements of the absolute photoabsorption cross sections of argon, krypton, and xenon using a double-ionization chamber and the Ne I (16.671 and 16.848 eV) and He I (21.218 eV) resonance lines. The absolute scales for the present low-resolution dipole (e,e) measurements have therefore been established by normalizing to the Samson and Yin values [28] at 21.218 eV for argon and krypton, and at 16.848 eV for xenon since at these energies there are no sharp structures in the respective photoabsorption cross sections.

The high-resolution dipole (e,e) spectrometer described in Refs. [49,91] with an impact energy of 3 keV and a mean scattering angle of 0° (acceptance angle of 3.0×10^{-5} sr) was used to obtain electron-energy-loss spectra (FWHM of 0.048 eV) of argon, krypton, and xenon in the energy-loss ranges 11–30, 9–30, and 8–30 eV, respectively, including the regions of the autoionizing structures due to excitation of inner-valence ms electrons. The Bethe-Born conversion factor of this high-resolution dipole (e,e) spectrometer has been determined by the procedures described earlier in parts I [49] and II [90] of this series of papers. The high-resolution electron-energy-loss spectra of argon, krypton, and xenon were multiplied by the instrumental Bethe-Born conversion factor to obtain relative optical oscillator strength spectra which were then normalized in the smooth continuum at 21.218 eV for argon and krypton, and at 16.848 eV for xenon using the absolute photoabsorption cross-section data recently reported by Samson and Yin [28].

For all the above measurements, the small contributions from the background gases remaining at the base pressure of the spectrometers (typically 2×10^{-7} Torr) were removed by subtracting the signal when the sample gas pressure was quartered. The energy scale of the low-resolution spectrometer was calibrated using the discrete excitation peaks at 11.828 eV for argon, 10.033 eV for krypton, and 8.437 eV for xenon, while the high-resolution spectra were calibrated by admitting helium simultaneously with the noble-gas sample and referencing to the $1\,^1S\rightarrow2\,^1P$ transition of helium which occurs at 21.218 eV [92]. No impurities were detected in the high-resolution electron-energy-loss spectra.

III. RESULTS AND DISCUSSIONS

A. Low-resolution measurements of the photoabsorption oscillator strengths for argon, krypton, and xenon

Relative photoabsorption spectra of argon, krypton, and xenon were obtained by Bethe-Born conversion of electron-energy-loss spectra measured with the low-resolution dipole (e,e) spectrometer from 10–500, 8–380, and 7–398 eV for argon, krypton, and xenon, respectively. The relative spectra were normalized at 21.218 eV for argon and krypton and at 16.848 eV for xenon using the recently published photoionization data of Samson and Yin [28]. The uncertainties of the present low-resolution dipole (e,e) work are estimated to be $\sim$5%. The results for argon, krypton, and xenon are presented in the following separate sections.

1. Low-resolution measurements for argon

Figures 1–3 show the presently measured absolute optical oscillator strengths for the photoabsorption of ar-

gon. The corresponding numerical values in the energy region 16–500 eV are summarized in Table I. Of the three noble gases (argon, krypton, and xenon) studied in the present work, the photoionization cross sections of argon have been previously studied in the greatest detail. Figures 1(a) and 1(b) show the presently measured absolute optical oscillator strengths for the valence-shell photoabsorption of argon in the energy region 10–60 eV along with previously reported experimental [16,19,23,25,26,33,93,94] and theoretical [2–9] data, respectively. In Fig. 1(a), the higher-resolution data from Samson [19] and Carlson *et al.* [23] in the 26–29 eV autoionizing region have been omitted to permit clearer comparison with the present low-resolution data. The data reported by Samson [19] and Carlson *et al.* [23] in the continuum autoionization regions will be compared with the present data obtained from the high-resolution dipole (e,e) spectrometer in Sec. III C. West and Marr [25] have made absolute photoabsorption measurements for argon over the range 36–310 eV and have given a critical evaluation of existing published cross-section data to obtain recommended (weighted-average) values throughout the vacuum ultraviolet and x-ray regions. These values [25,26] did not take into account previously published data in the autoionizing region (26–29 eV) and

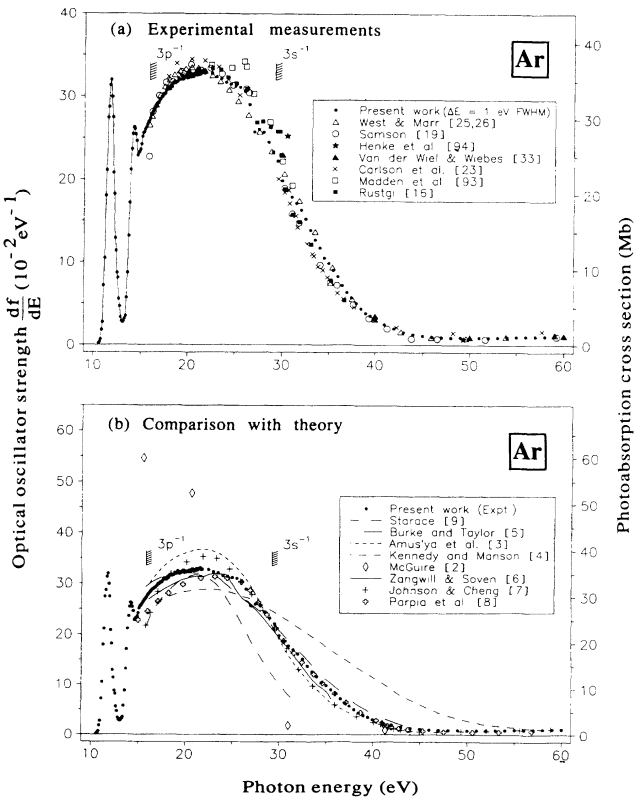

FIG. 1. Absolute oscillator strengths for the photoabsorption of argon in the energy region 10–60 eV. (a) Comparison with other experimental data [16,19,23,25,26,33,93,94]. The discrete region below 16 eV is shown at high resolution in Fig. 9. The resonances in the region 26–29.2 eV preceding the $3s^{-1}$ edge are shown at high resolution in Fig. 14. (b) Comparison with theory [2–9].

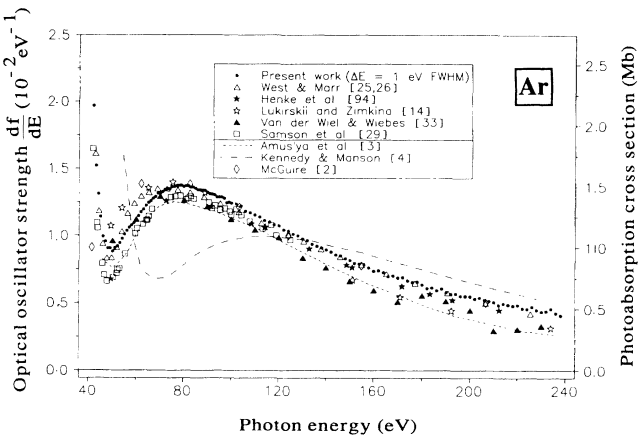

FIG. 2. Absolute oscillator strengths for the photoabsorption of argon in the energy region 40–240 eV compared with other experimental [14,25,26,29,33,94] and theoretical [2–4] data.

simply reported interpolated smooth cross sections throughout the autoionizing region. From Fig. 1(a) it can be seen that all the experimental data including the present low-resolution results show a similar shape for the continuum and are in generally good quantitative agreement. The data from Madden, Ederer, and Codling [93] are slightly higher than other experimental values in the vicinity of 25 eV. In contrast to the experimental data, the theoretical values for argon show substantial differences in terms of both the shape and the absolute values of the cross sections when compared with the present results [see Fig. 1(b)]. The one-electron calculation by McGuire [2] gives much higher cross sections just above the $3p$ threshold and the cross sections drop very quickly to a very low value before reaching the Cooper minimum at ~ 50 eV. Even with the inclusion of electron correlation, the calculations reported by Starace [9] and by Kennedy and Manson [4] still show large discrepancies with the present and other measured values. Since relativistic effects in argon are small, the RPAE calculation of Amus'ya, Cherepkov, and Chernysheva [3] and the relativistic RPAE of Johnson and Cheng [7] agree

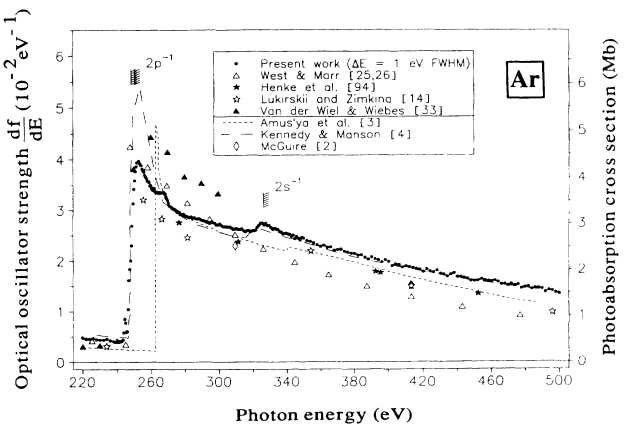

FIG. 3. Absolute oscillator strengths for the photoabsorption of argon in the energy region 220–500 eV compared with other experimental [14,25,26,33,94] and theoretical [2–4] data.

TABLE I. Absolute optical oscillator strengths for the photoabsorption of argon above the first ionization potential obtained using the low-resolution (1 eV FWHM) dipole (e,e) spectrometer (16–500 eV).

Energy (eV)	Oscillator strength (10^{-2} eV^{-1})	Energy (eV)	Oscillator strength (10^{-2} eV^{-1})	Energy (eV)	Oscillator strength (10^{-2} eV^{-1})	Energy (eV)	Oscillator strength (10^{-2} eV^{-1})
16.0	27.74	21.7	32.80	60.0	1.110	134.0	0.936
16.1	27.96	21.8	32.86	61.0	1.146	136.0	0.920
16.2	28.16	22.5	32.90	62.0	1.175	138.0	0.910
16.3	28.48	23.0	32.36	63.0	1.196	140.0	0.895
16.4	28.55	23.5	32.16	64.0	1.223	142.0	0.879
16.5	28.94	24.0	31.66	65.0	1.245	144.0	0.857
16.6	28.95	24.5	31.49	66.0	1.259	146.0	0.851
16.7	29.25	25.0	31.24	67.0	1.278	148.0	0.829
16.8	29.25	25.5	31.08	68.0	1.290	150.0	0.816
16.9	29.52	26.0	30.63	69.0	1.314	152.0	0.793
17.0	29.71	26.5	29.02	70.0	1.316	154.0	0.789
17.1	29.99	27.0	25.76	71.0	1.325	156.0	0.784
17.2	29.97	27.5	26.06	72.0	1.341	158.0	0.762
17.3	30.30	28.0	25.71	73.0	1.347	160.0	0.737
17.4	30.25	28.5	24.50	74.0	1.348	162.0	0.740
17.5	30.39	29.0	23.37	75.0	1.364	164.0	0.726
17.6	30.73	29.5	22.24	76.0	1.365	166.0	0.696
17.7	31.05	30.0	19.84	77.0	1.373	168.0	0.701
17.8	31.09	30.5	18.66	78.0	1.374	170.0	0.687
17.9	30.86	31.0	17.85	79.0	1.376	172.0	0.689
18.0	30.87	31.5	17.08	80.0	1.366	174.0	0.665
18.1	31.33	32.0	16.25	81.0	1.371	176.0	0.654
18.2	31.15	32.5	15.19	82.0	1.371	178.0	0.658
18.3	31.57	33.0	13.81	83.0	1.359	180.0	0.636
18.4	31.67	33.5	12.69	84.0	1.363	182.0	0.609
18.5	31.81	34.0	11.73	85.0	1.353	184.0	0.614
18.6	31.61	34.5	10.50	86.0	1.341	186.0	0.593
18.7	31.73	35.0	9.89	87.0	1.340	188.0	0.606
18.8	31.78	35.5	9.02	88.0	1.338	190.0	0.579
18.9	32.19	36.0	8.28	89.0	1.337	192.0	0.566
19.0	32.03	36.5	7.20	90.0	1.322	194.0	0.569
19.1	32.02	37.0	6.34	91.0	1.312	196.0	0.552
19.2	32.51	37.5	5.71	92.0	1.310	198.0	0.550
19.3	32.41	38.0	5.04	93.0	1.304	200.0	0.548
19.4	32.02	38.5	4.38	94.0	1.288	202.0	0.530
19.5	32.19	39.0	3.84	95.0	1.288	204.0	0.538
19.6	32.35	39.5	3.51	96.0	1.288	206.0	0.521
19.7	32.52	40.0	3.03	97.0	1.278	208.0	0.514
19.8	32.71	41.0	2.48	98.0	1.244	210.0	0.506
19.9	32.23	42.0	1.970	99.0	1.248	212.0	0.485
20.0	32.49	43.0	1.521	100.0	1.241	214.0	0.495
20.1	32.51	44.0	1.312	102.0	1.236	216.0	0.487
20.2	32.36	45.0	1.141	104.0	1.219	218.0	0.480
20.3	32.38	46.0	0.991	106.0	1.182	220.0	0.484
20.4	32.71	47.0	0.956	108.0	1.171	222.0	0.459
20.5	32.40	48.0	0.905	110.0	1.154	224.0	0.455
20.6	32.58	49.0	0.906	112.0	1.139	226.0	0.470
20.7	32.91	50.0	0.883	114.0	1.112	228.0	0.446
20.8	32.94	51.0	0.909	116.0	1.101	230.0	0.436
20.9	32.57	52.0	0.923	118.0	1.081	232.0	0.439
21.0	32.75	53.0	0.946	120.0	1.074	234.0	0.457
21.1	32.62	54.0	0.977	122.0	1.043	236.0	0.425
21.2[a]	33.00	55.0	1.009	124.0	1.035	238.0	0.408
21.3	32.72	56.0	1.036	126.0	1.011	240.0	0.405
21.4	32.89	57.0	1.059	128.0	0.999	240.5	0.412
21.5	33.09	58.0	1.078	130.0	0.975	241.0	0.404
21.6	33.16	59.0	1.094	132.0	0.963	241.5	0.402

TABLE I. (*Continued.*)

Energy (eV)	Oscillator strength (10^{-2} eV^{-1})	Energy (eV)	Oscillator strength (10^{-2} eV^{-1})	Energy (eV)	Oscillator strength (10^{-2} eV^{-1})	Energy (eV)	Oscillator strength (10^{-2} eV^{-1})
242.0	0.409	270.0	3.19	316.0	2.57	392.0	2.03
242.5	0.406	270.5	3.14	317.0	2.59	394.0	2.01
243.0	0.416	271.0	3.08	318.0	2.59	396.0	1.971
243.5	0.439	271.5	3.07	319.0	2.57	398.0	2.01
244.0	0.578	272.0	3.07	320.0	2.59	400.0	1.983
244.5	0.849	272.5	3.04	321.0	2.59	402.0	1.898
245.0	0.774	273.0	3.03	322.0	2.60	404.0	1.931
245.5	0.593	273.5	3.02	323.0	2.66	406.0	1.917
246.0	0.609	274.0	3.02	324.0	2.70	408.0	1.869
246.5	1.049	274.5	3.01	325.0	2.74	410.0	1.891
247.0	1.615	275.0	2.99	326.0	2.74	412.0	1.875
247.5	1.838	275.5	2.96	327.0	2.70	414.0	1.854
248.0	2.00	276.0	2.97	328.0	2.74	416.0	1.839
248.5	2.30	276.5	2.96	329.0	2.69	418.0	1.820
249.0	2.69	277.0	2.96	330.0	2.69	420.0	1.778
249.5	3.13	277.5	2.91	331.0	2.65	422.0	1.827
250.0	3.42	278.0	2.92	332.0	2.61	424.0	1.784
250.5	3.59	278.5	2.91	333.0	2.64	426.0	1.769
251.0	3.77	279.0	2.90	334.0	2.62	428.0	1.805
251.5	3.86	279.5	2.92	335.0	2.61	430.0	1.743
252.0	3.94	280.0	2.89	336.0	2.58	432.0	1.724
252.5	3.94	281.0	2.88	337.0	2.56	434.0	1.686
253.0	3.97	282.0	2.87	338.0	2.52	436.0	1.728
253.5	3.93	283.0	2.85	339.0	2.54	438.0	1.751
254.0	3.90	284.0	2.87	340.0	2.54	440.0	1.677
254.5	3.89	285.0	2.84	341.0	2.52	442.0	1.675
255.0	3.81	286.0	2.85	342.0	2.52	444.0	1.655
255.5	3.78	287.0	2.83	343.0	2.48	446.0	1.637
256.0	3.76	288.0	2.83	344.0	2.50	448.0	1.601
256.5	3.69	289.0	2.83	345.0	2.43	450.0	1.604
257.0	3.65	290.0	2.81	346.0	2.47	452.0	1.606
257.5	3.63	291.0	2.79	347.0	2.44	454.0	1.635
258.0	3.58	292.0	2.79	348.0	2.41	456.0	1.608
258.5	3.57	293.0	2.77	349.0	2.46	458.0	1.597
259.0	3.55	294.0	2.76	350.0	2.44	460.0	1.587
259.5	3.48	295.0	2.74	352.0	2.40	462.0	1.605
260.0	3.49	296.0	2.76	354.0	2.38	464.0	1.578
260.5	3.43	297.0	2.75	356.0	2.35	466.0	1.528
261.0	3.40	298.0	2.74	358.0	2.31	468.0	1.532
261.5	3.44	299.0	2.71	360.0	2.28	470.0	1.507
262.0	3.39	300.0	2.71	362.0	2.30	472.0	1.532
262.5	3.38	301.0	2.73	364.0	2.27	474.0	1.501
263.0	3.36	302.0	2.70	366.0	2.27	476.0	1.523
263.5	3.35	303.0	2.67	368.0	2.21	478.0	1.453
264.0	3.36	304.0	2.67	370.0	2.22	480.0	1.471
264.5	3.34	305.0	2.67	372.0	2.22	482.0	1.482
265.0	3.36	306.0	2.66	374.0	2.18	484.0	1.436
265.5	3.34	307.0	2.67	376.0	2.17	486.0	1.454
266.0	3.34	208.0	2.64	378.0	2.14	488.0	1.452
266.5	3.35	309.0	2.62	380.0	2.14	490.0	1.437
267.0	3.35	310.0	2.63	382.0	2.11	492.0	1.374
267.5	3.36	311.0	2.63	384.0	2.11	494.0	1.411
268.0	3.34	312.0	2.62	386.0	2.06	496.0	1.400
268.5	3.33	313.0	2.62	388.0	2.03	498.0	1.364
269.0	3.27	314.0	2.63	390.0	2.07	500.0	1.346
269.5	3.22	315.0	2.59				

[a]Normalized to Ref. [28] at 21.218 eV. σ (Mb) $= 109.75 df/dE$ (eV^{-1}).

very closely with each other. However, these calculations [3,7] are considerably higher than the present and other experimental values below 30 eV and are somewhat lower in the energy region 30–50 eV. The values reported by Parpia, Johnson, and Radojevic [8] using the relativistic time-dependent local-density approximation (RTDLDA) method give excellent agreement with the presently reported experimental values above 25 eV, but in common with most of the other theoretical work there still exist some discrepancies with the experimental data in the energy region between the $3p$ threshold and the cross-section maximum.

Figure 2 shows the presently measured absolute photoabsorption oscillator strengths for argon from 40 to 240 eV just below the inner-shell $2p$ excitations of argon. Other previously reported experimental and theoretical data that are available in this energy region are also shown for comparison. The present data are in generally good agreement with the compilation data reported by Henke *et al.* [94] and West and Marr [25,26]. The photoabsorption data of Lukirskii and Zimkina [14] and the earlier electron-impact data of Van der Wiel and Wiebes [33] give lower values at energies above 120 eV. The values measured recently by Samson *et al.* [29] using a double-ionization chamber in the energy region 40–120 eV are slightly lower than the present work. In theoretical work, the one-electron calculation of McGuire [2] which shows very high cross sections just above the $3p$ threshold [Fig. 1(b)] gives very good agreement with the present results from an energy just above the Cooper minimum to 240 eV (Fig. 2). The RPAE calculations reported by Amus'ya, Cherepkov, and Chernysheva [3] show a similar shape in the continuum to the present measurements, but the theoretical values are slightly lower from 40 to 150 eV and become increasingly lower above 150 eV. The photoionization cross sections calculated by Kennedy and Manson [4] show large discrepancies with the present and all other experimental data and, furthermore, the predicted position of the Cooper minimum is ~15 eV too high in energy.

Figure 3 shows the presently measured absolute photoabsorption oscillator strengths for argon in the energy region from 220 to 500 eV where excitation of the argon $2s$ and $2p$ electrons take place on top of the valence-shell continuum. The limited previously published experimental and theoretical data in this energy region are also shown in Fig. 3 for comparison. Unlike the situation below 240 eV, the agreement between the available experimental data is poor in this energy region. It can be seen in Fig. 3 that the data reported by Lukirskii and Zimkina [14] and the compilation data of Henke *et al.* [94] are ~10–25 % lower than the present results. The data of West and Marr [25,26], which are slightly higher than the presently reported values in the energy region 250–290 eV, are lower by more than 30% at energies above 320 eV. The theoretical calculations reported by Kennedy and Manson [4], which show considerable discrepancies with the experimental data below 240 eV, exhibit very good agreement with the presently measured values in the energy region 270–500 eV, while the calculations of Amus'ya, Cherepkov, and Chernysheva [3] and

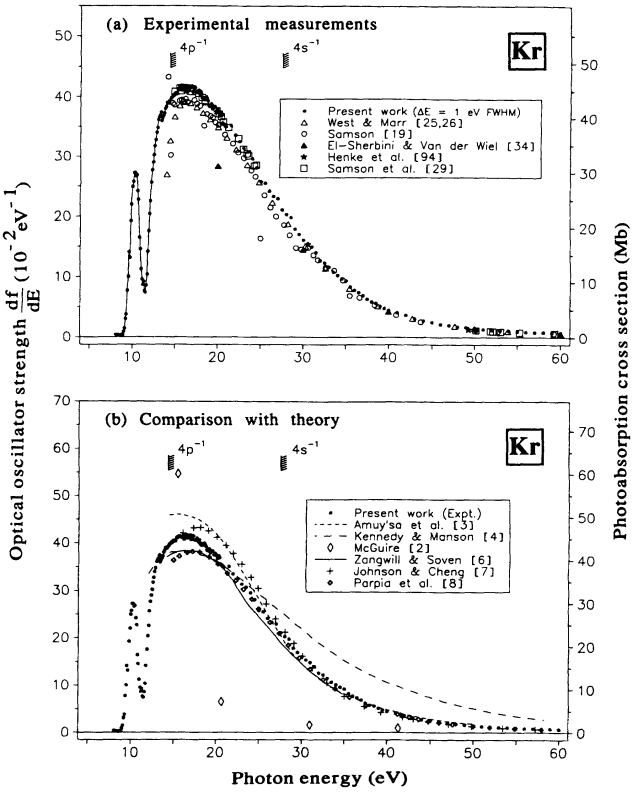

FIG. 4. Absolute oscillator strengths for the photoabsorption of krypton in the energy region 5–60 eV. (a) Comparison with other experimental data [19,25,26,34,94]. The discrete region below 15 eV is shown at high resolution in Fig. 10. The resonances in the region 24.5–27.5 eV preceding the $4s^{-1}$ edge are shown at high resolution in Fig. 15. (b) Comparison with theory [2–4,6–8].

of McGuire [2] are (~10–15 %) lower than the present results in this energy region.

2. *Low-resolution measurements for krypton*

Figures 4 and 5 show the presently measured absolute optical oscillator strengths for the photoabsorption of krypton and Table II summarizes the numerical absolute

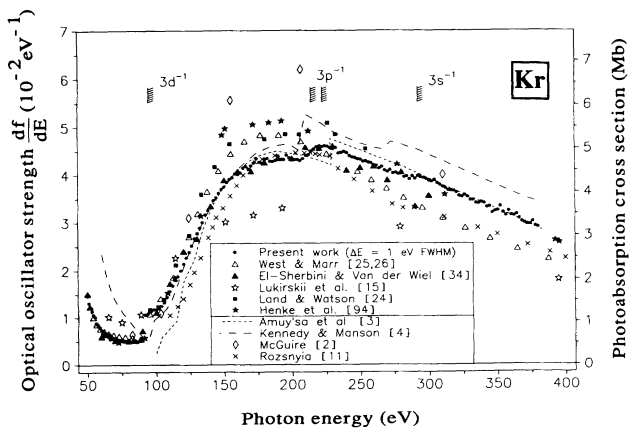

FIG. 5. Absolute oscillator strengths for the photoabsorption of krypton in the energy region 50–400 eV compared with other experimental [15,24–26,34,94] and theoretical [2–4,11] data.

TABLE II. Absolute optical oscillator strengths for the photoabsorption of krypton above the first ionization potential obtained using the low resolution (1 eV FWHM) dipole (e,e) spectrometer (14.7–380 eV).

Energy (eV)	Oscillator strength (10^{-2} eV^{-1})	Energy (eV)	Oscillator strength (10^{-2} eV^{-1})	Energy (eV)	Oscillator strength (10^{-2} eV^{-1})	Energy (eV)	Oscillator strength (10^{-2} eV^{-1})
14.7	40.22	20.3	37.33	51.0	1.319	144.0	3.53
14.8	40.16	20.4	36.98	52.0	1.220	146.0	3.62
14.9	40.56	20.5	35.65	53.0	1.135	148.0	3.70
15.0	40.42	20.6	35.42	54.0	1.057	150.0	3.75
15.1	40.64	20.7	35.39	55.0	1.014	152.0	3.84
15.2	40.50	20.8	35.09	56.0	0.880	154.0	3.91
15.3	41.25	20.9	35.03	57.0	0.862	156.0	3.94
15.4	41.13	21.0[a]	34.90	58.0	0.818	158.0	4.02
15.5	41.41	21.5	35.15	59.0	0.788	160.0	4.01
15.6	41.46	22.0	33.57	60.0	0.737	162.0	4.05
15.7	41.49	22.5	32.49	61.0	0.722	164.0	4.14
15.8	41.22	23.0	31.38	62.0	0.679	166.0	4.18
15.9	41.28	23.5	30.79	63.0	0.657	168.0	4.12
16.0	41.20	24.0	29.62	64.0	0.667	170.0	4.19
16.1	41.73	24.5	28.12	65.0	0.599	172.0	4.25
16.2	40.78	25.0	25.81	66.0	0.645	174.0	4.35
16.3	41.57	25.5	25.57	67.0	0.605	176.0	4.27
16.4	41.41	26.0	24.22	68.0	0.582	178.0	4.25
16.5	41.81	26.5	23.37	69.0	0.553	180.0	4.32
16.6	41.04	27.0	22.99	70.0	0.551	182.0	4.35
16.7	41.46	27.5	21.14	72.0	0.527	184.0	4.29
16.8	41.62	28.0	20.38	74.0	0.528	186.0	4.28
16.9	41.76	28.5	19.85	76.0	0.505	188.0	4.31
17.0	40.77	29.0	17.92	78.0	0.499	190.0	4.40
17.1	41.02	29.5	17.04	80.0	0.494	192.0	4.33
17.2	41.63	30.0	16.08	82.0	0.497	194.0	4.32
17.3	41.53	30.5	15.47	84.0	0.494	196.0	4.41
17.4	40.70	31.0	14.96	86.0	0.489	198.0	4.36
17.5	40.67	31.5	14.01	88.0	0.508	200.0	4.31
17.6	40.65	32.0	12.69	90.0	0.565	202.0	4.32
17.7	41.07	32.5	12.30	92.0	1.064	204.0	4.32
17.8	40.70	33.0	11.58	94.0	1.088	206.0	4.30
17.9	40.26	33.5	10.78	96.0	1.138	208.0	4.34
18.0	40.70	34.0	10.20	98.0	1.170	210.0	4.41
18.1	39.82	34.5	9.69	100.0	1.171	212.0	4.43
18.2	39.96	35.0	9.30	102.0	1.199	214.0	4.50
18.3	39.55	35.5	8.33	104.0	1.252	216.0	4.54
18.4	39.65	36.0	7.77	106.0	1.327	218.0	4.59
18.5	39.58	36.5	7.39	108.0	1.444	220.0	4.61
18.6	40.00	37.0	6.92	110.0	1.566	222.0	4.59
18.7	39.64	37.5	6.28	112.0	1.684	224.0	4.61
18.8	39.35	38.0	5.85	114.0	1.797	226.0	4.60
18.9	38.59	38.5	5.65	116.0	1.878	228.0	4.57
19.0	38.40	39.0	5.15	118.0	2.00	230.0	4.55
19.1	38.53	39.5	4.81	120.0	2.14	232.0	4.57
19.2	38.83	40.0	4.47	122.0	2.27	234.0	4.46
19.3	37.98	41.0	4.10	124.0	2.38	236.0	4.46
19.4	38.41	42.0	3.66	126.0	2.52	238.0	4.49
19.5	38.32	43.0	3.12	128.0	2.67	240.0	4.46
19.6	38.38	44.0	2.74	130.0	2.78	242.0	4.40
19.7	37.57	45.0	2.49	132.0	2.89	244.0	4.37
19.8	37.76	46.0	2.17	134.0	3.01	246.0	4.36
19.9	37.85	47.0	1.983	136.0	3.17	248.0	4.34
20.0	37.46	48.0	1.787	138.0	3.26	250.0	4.32
20.1	36.80	49.0	1.675	140.0	3.33	252.0	4.28
20.2	36.79	50.0	1.475	142.0	3.47	254.0	4.29

TABLE II. (*Continued.*)

Energy (eV)	Oscillator strength (10^{-2} eV^{-1})	Energy (eV)	Oscillator strength (10^{-2} eV^{-1})	Energy (eV)	Oscillator strength (10^{-2} eV^{-1})	Energy (eV)	Oscillator strength (10^{-2} eV^{-1})
256.0	4.26	288.0	3.98	320.0	3.63	352.0	3.34
258.0	4.25	290.0	3.92	322.0	3.56	354.0	3.21
260.0	4.21	292.0	3.98	324.0	3.54	356.0	3.15
262.0	4.20	294.0	3.95	326.0	3.58	358.0	3.25
264.0	4.14	296.0	3.94	328.0	3.54	360.0	3.16
266.0	4.17	298.0	3.92	330.0	3.48	362.0	3.14
268.0	4.09	300.0	3.88	332.0	3.48	364.0	3.17
270.0	4.07	302.0	3.86	334.0	3.41	366.0	3.09
272.0	4.11	304.0	3.90	336.0	3.40	368.0	3.02
274.0	4.04	306.0	3.83	338.0	3.43	370.0	3.00
276.0	4.05	308.0	3.79	340.0	3.41	372.0	2.97
278.0	4.01	310.0	3.75	342.0	3.33	374.0	2.97
280.0	4.03	312.0	3.73	344.0	3.34	376.0	3.02
282.0	3.96	314.0	3.68	346.0	3.21	378.0	2.93
284.0	3.97	316.0	3.68	348.0	3.24	380.0	2.91
286.0	3.91	318.0	3.67	350.0	3.25		

[a]Normalized to Ref. [28] at 21.218 eV. σ (Mb) $= 109.75 df/dE$ (eV^{-1}).

oscillator strength values in the energy region 14.7–380 eV. In Figs. 4(a) and 4(b) the presently measured valence-shell photoabsorption oscillator strengths for krypton in the energy region 5–60 eV are compared with the previously reported experimental and theoretical values, respectively. The earlier reported photoionization data of Samson [19] are slightly lower than the present work in the energy region from the $4p$ threshold to 30 eV. The weighted-average values reported in the West and Marr compilation [25,26], which included the data from Samson [19], show similar behavior to the original Samson data [19]. In contrast, the most recent data reported by Samson *et al.* [29] show excellent agreement with the presently reported values. As shown in Fig. 4(b), the situation for the theoretical cross sections of krypton when compared with the experimental data is similar to that for argon [in Fig. 1(b)]. Even though agreement between theoretical and experimental values is better at higher energies, difficulties still remain in describing the behavior of the photoionization cross sections just above the $4p$ threshold and in the region around the cross-section maximum.

Ionization from the $3d$ subshell of krypton takes place at ~90 eV. The ejection of the d electrons is delayed due to the angular-momentum barrier which separates the inner-well and outer-well states. The photoionization cross sections reach a maximum value at ~180 eV which is ~90 eV above threshold. Figure 5 shows the presently measured photoabsorption cross sections of krypton in the energy region 50–400 eV, which includes not only the $3d$ ionization threshold but also the $3s$ (~290 eV) and $3p$ (~220 eV) thresholds as well. The optical data of West and Marr [25,26], Land and Watson [24], and Henke *et al.* [94] show 10–15 % higher values than the present work around the $3d$ cross-section maximum, while the values of Lukirskii, Brytov, and Zimkina [15] are lower by more than 25%. The electron-impact data of El-Sherbini and Van der Wiel [34] agree very well with the present work. The one-electron calculation of McGuire [2] gives cross sections which are too high. In contrast all theoretical calculations which include electron correlation [3,4,11] adequately describe the behavior of the photoionization oscillator strength of the $3d$ electrons. In particular, the RPAE data of Amus'ya, Cherepkov, and Chernysheva [3] show extremely good agreement with the present data.

3. *Low-resolution measurements for xenon*

Figures 6–8 show the presently measured absolute optical oscillator strengths for the photoabsorption of xenon and Table III summarizes the corresponding absolute oscillator strength values in the energy region 13.5–398 eV. Figures 6(a) and 6(b) show the presently measured photoabsorption oscillator strengths for xenon in the energy region 5–60 eV along with previously reported experimental and theoretical data, respectively. It can be seen from Fig. 6(a) that the present data are in excellent agreement with the recent work of Samson *et al.* [29] over the entire energy range shown. The data from the West and Morton compilation [27] are much higher than the present work just above the $5p$ threshold but are very close to the present data at 20 eV. The earlier reported Samson data [19] are slightly lower in the region 16–30 eV. In theoretical work, the relativistic RPAE data of Johnson and Cheng [7] show better agreement with the present work than do the nonrelativistic RPAE data of Amus'ya, Cherepkov, and Chernysheva [3], which give much higher cross sections just above the $5p$ threshold. The calculations reported by Zangwill and Soven [6] in the 15–25 eV region using density-functional theory show very good agreement with the present work. In contrast,

other theoretical calculations yield less satisfactory results, particularly below 20 eV.

Photoionization cross sections for the 4*d* subshell of xenon have been studied extensively both experimentally and theoretically. Figures 7(a) and 7(b) show the presently measured photoabsorption oscillator strengths of xenon in the energy region 40–200 eV. It can be seen from Fig. 7(a) that the values obtained in the present work are slightly lower than other experimental data in the energy region around the 4*d* ionization cross-section maximum. The data from Lukirskii, Brytov, and Zimkina [15], Ederer [17], and El-Sherbini and Van der Wiel [34] give the highest oscillator strengths in this region. All one-electron calculations [2,10] are in severe disagreement with experiment and are not shown in Fig. 7(b). This disagreement is not surprising in view of the many-electron effects which influence the 4*d* cross sections. The more complex calculations [3,4,6,8,9,11] which include electron correlation achieve closer agreement with experimental values. In Fig. 7(b) it can be seen that the theoretical calculations, including electron correlation, give photoionization cross sections reasonably similar in shape to the present experimental work. However, the cross-section maxima reported by Starace [9], Kennedy and Manson [4], and Rozsnyai [11] are shifted to higher

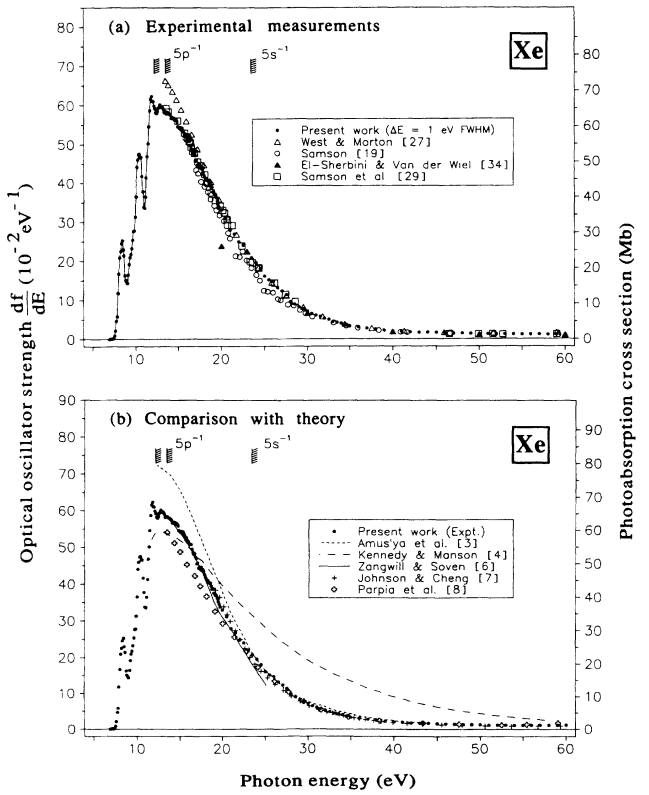

FIG. 6. Absolute oscillator strengths for the photoabsorption of xenon in the energy region 5–60 eV. (a) Comparison with other experimental data [19,27,29,34]. The discrete region below 13.5 eV is shown at high resolution in Fig. 12. The resonances in the region 20.5–27.4 eV preceding the $5s^{-1}$ edge are shown at high resolution in Fig. 16. (b) Compared with theory [3,4,6–8]

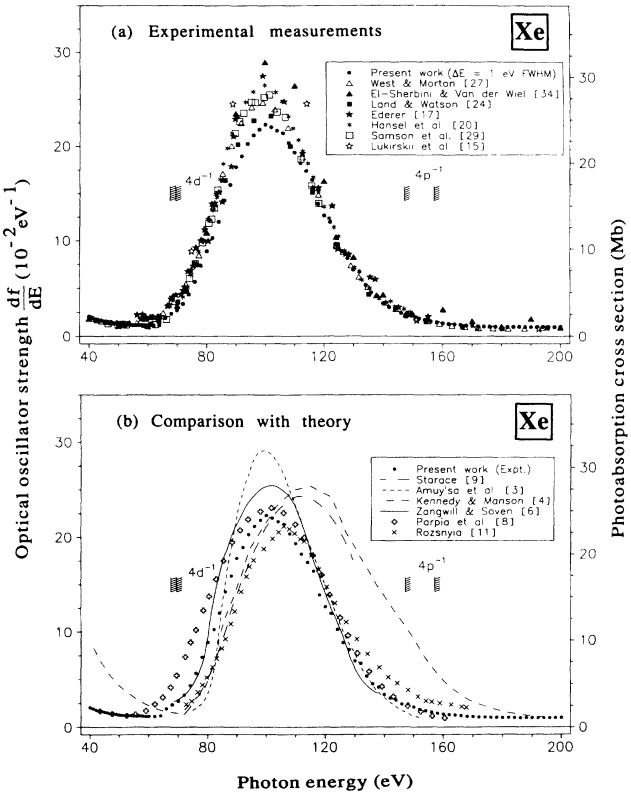

FIG. 7. Absolute oscillator strengths for the photoabsorption of xenon in the energy region 40–200 eV. (a) Comparison with other experimental data [15,17,20,27,29,34]. (b) Comparison with theory [3,4,6,8,9,11].

energy. The calculations reported by Zangwill and Soven [6] and Parpia, Johnson, and Radojevic [8] show reasonable agreement with the present work, although the calculated values are slightly higher.

Figure 8 shows the presently determined photoabsorption oscillator strengths for xenon in the energy region 160–398 eV. There are few previously reported data in this energy region. The data from the West and Morton

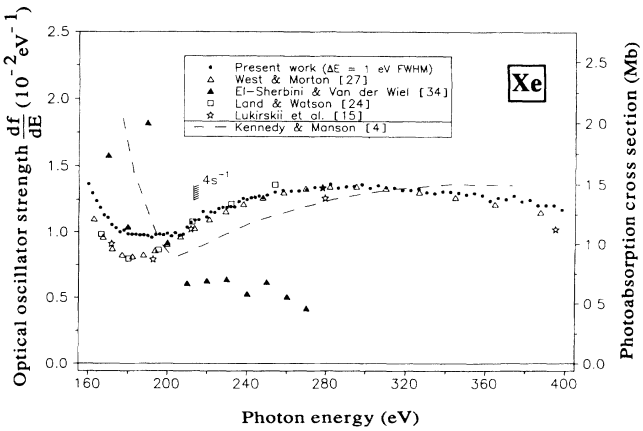

FIG. 8. Absolute oscillator strengths for the photoabsorption of xenon in the energy region 160–400 eV compared with other experimental [15,24,27,34] and theoretical [4] data.

TABLE III. Absolute optical oscillator strengths for the photoabsorption of xenon above the first ionization potential obtained using the low-resolution (1 eV FWHM) dipole (e,e) spectrometer (13.5–398 eV).

Energy (eV)	Oscillator strength (10^{-2} eV^{-1})	Energy (eV)	Oscillator strength (10^{-2} eV^{-1})	Energy (eV)	Oscillator strength (10^{-2} eV^{-1})	Energy (eV)	Oscillator strength (10^{-2} eV^{-1})
13.5	58.35	19.1	37.49	54.0	1.201	160.0	1.366
13.6	58.29	19.2	37.00	55.0	1.160	162.0	1.297
13.7	57.96	19.3	36.96	56.0	1.153	164.0	1.241
13.8	57.98	19.4	36.19	57.0	1.178	166.0	1.189
13.9	57.80	19.5	35.28	58.0	1.145	168.0	1.130
14.0	57.53	19.6	34.60	59.0	1.137	170.0	1.111
14.1	56.71	19.7	33.83	60.0	1.148	172.0	1.056
14.2	56.95	20.0	33.04	62.0	1.124	174.0	1.031
14.3	56.62	20.5	31.21	64.0	1.177	176.0	0.999
14.4	56.86	21.0	27.93	66.0	1.900	178.0	1.015
14.5	56.34	21.5	26.88	68.0	2.33	180.0	0.986
14.6	56.58	22.0	24.88	70.0	2.71	182.0	0.983
14.7	56.34	22.5	24.01	72.0	3.36	184.0	0.982
14.8	55.87	23.0	22.08	74.0	4.36	186.0	0.977
14.9	54.59	23.5	20.84	76.0	5.66	188.0	0.977
15.0	54.47	24.0	19.62	78.0	7.38	190.0	0.972
15.1	54.16	24.5	18.13	80.0	8.92	192.0	0.960
15.2	54.37	25.0	16.17	82.0	10.29	194.0	0.981
15.3	53.74	25.5	15.22	84.0	11.99	196.0	0.984
15.4	54.25	26.0	14.78	86.0	14.25	198.0	0.979
15.5	53.62	26.5	13.20	88.0	15.91	200.0	0.990
15.6	53.16	27.0	12.39	90.0	17.80	202.0	0.969
15.7	52.20	27.5	11.39	92.0	18.96	204.0	0.995
15.8	52.65	28.0	9.59	94.0	20.30	206.0	0.974
15.9	51.86	28.5	8.97	96.0	21.19	208.0	0.983
16.0	51.64	29.0	8.27	98.0	21.83	210.0	1.037
16.1	51.07	29.5	7.72	100.0	22.33	212.0	1.072
16.2	50.88	30.0	7.17	102.0	22.05	214.0	1.090
16.3	50.84	30.5	6.54	104.0	21.67	216.0	1.092
16.4	49.54	31.0	6.12	106.0	21.41	218.0	1.159
16.5	48.68	31.5	5.80	108.0	20.40	220.0	1.114
16.6	48.20	32.0	5.28	110.0	19.37	222.0	1.154
16.7	48.41	32.5	4.95	112.0	18.23	224.0	1.151
16.8[a]	47.44	33.0	4.48	114.0	17.39	226.0	1.181
16.9	47.11	33.5	4.26	116.0	16.45	228.0	1.190
17.0	45.63	34.0	4.02	118.0	13.91	230.0	1.188
17.1	45.82	34.5	3.69	120.0	12.66	232.0	1.197
17.2	44.48	35.0	3.28	122.0	11.96	234.0	1.194
17.3	44.70	36.0	3.11	124.0	10.29	236.0	1.235
17.4	44.16	37.0	2.77	126.0	8.90	238.0	1.258
17.5	44.74	38.0	2.49	128.0	8.15	240.0	1.248
17.6	43.80	39.0	2.23	130.0	6.94	242.0	1.263
17.7	44.09	40.0	2.05	132.0	6.73	244.0	1.267
17.8	43.58	41.0	1.944	134.0	5.36	246.0	1.277
17.9	42.73	42.0	1.789	136.0	4.55	248.0	1.265
18.0	42.01	43.0	1.696	138.0	4.19	250.0	1.284
18.1	41.44	44.0	1.664	140.0	3.41	254.0	1.305
18.2	40.88	45.0	1.578	142.0	3.03	258.0	1.319
18.3	41.07	46.0	1.493	144.0	2.82	262.0	1.315
18.4	40.62	47.0	1.407	146.0	2.43	266.0	1.315
18.5	40.43	48.0	1.398	148.0	2.41	270.0	1.323
18.6	40.28	49.0	1.341	150.0	2.11	274.0	1.342
18.7	39.55	50.0	1.314	152.0	1.838	278.0	1.341
18.8	38.70	51.0	1.243	154.0	1.702	282.0	1.365
18.9	38.84	52.0	1.219	156.0	1.554	286.0	1.339
19.0	37.61	53.0	1.203	158.0	1.454	290.0	1.347

TABLE III. (*Continued.*)

Energy (eV)	Oscillator strength (10^{-2} eV^{-1})	Energy (eV)	Oscillator strength (10^{-2} eV^{-1})	Energy (eV)	Oscillator strength (10^{-2} eV^{-1})	Energy (eV)	Oscillator strength (10^{-2} eV^{-1})
294.0	1.350	322.0	1.322	350.0	1.288	378.0	1.237
298.0	1.363	326.0	1.332	354.0	1.300	382.0	1.249
302.0	1.337	330.0	1.306	358.0	1.283	386.0	1.208
306.0	1.356	334.0	1.297	362.0	1.241	390.0	1.207
310.0	1.340	338.0	1.313	366.0	1.264	394.0	1.208
314.0	1.338	342.0	1.309	370.0	1.254	398.0	1.175
318.0	1.321	346.0	1.302	374.0	1.279		

[a]Normalized to Ref. [28] at 16.848 eV. σ (Mb)$=109.75 df/dE$ (eV^{-1}).

compilation [27] are lower than the present values in the energy region 160–200 eV but show good agreement with the present work at higher energies. Similar to the results obtained from the data reported by Lukirskii and Zimkina [14] for argon and by Lukirskii, Brytov, and Zimkina [15] for krypton, the data reported by Lukirskii Brytov, and Zimkina [15] for xenon are lower than the present values at energies higher than 160 eV. The earlier dipole electron-impact data of El-Sherbini and Van der Wiel [34] show large statistical errors in this energy region, and are much lower than the present work above 200 eV. The calculation by Kennedy and Manson [4], also shown in Fig. 8, shows fair agreement with experiment above 200 eV.

B. High-resolution measurements of the photoabsorption oscillator strengths for the discrete transitions below the *mp* ionization thresholds for argon ($m=3$), krypton ($m=4$), and xenon ($m=5$)

High-resolution electron-energy-loss spectra at resolutions of 0.048, 0.072, and 0.098 eV FWHM in the energy ranges 11–22 eV for argon, 9–22 eV for krypton, and 8–22 eV for xenon were multiplied by the appropriate Bethe-Born factors for the high-resolution dipole (e,e) spectrometer (see part I [49] and part II [90]) to obtain relative optical oscillator strength spectra which were then normalized in the smooth continuum regions at 21.218 eV for argon and krypton, and at 16.848 eV for xenon using the absolute data determined by Samson and Yin [28]. Figures 9–13 show the resulting absolute differential optical oscillator strength spectra of argon, krypton, and xenon at a resolution of 0.048-eV FWHM. The dipole-allowed electronic transitions from the ms^2mp^6 configurations of argon, krypton, and xenon with $m=3$, 4, and 5, respectively, to members of the $ms^2mp^5(^2P_{3/2,1/2})ns$ and nd manifolds (where $n>m$) were observed. The positions and assignments [95] of the various members of the nl and nl' series are indicated in the figures where the $nd[1/2]$ and $nd[3/2]$ states which converge to the same $^2P_{3/2}$ limit are labeled as nd and $n\underline{d}$, respectively. For peaks in the experimental spectrum which are completely resolved, such as the $4s$ and $4s'$ resonance lines of argon, integration of the peak areas provides a direct measure of the absolute optical oscillator strengths for the respective individual discrete electronic transitions. For states at higher energies which cannot be completely resolved, absolute oscillator strengths have been obtained from fitted peak areas as shown in the figures, according to least-squares fits of the experimental data. The same fitting procedures have been applied to the spectra obtained at the three different experimental resolutions. The consistency of the oscillator strength values obtained for given transitions at the different resolutions confirms the accuracy of the fitting procedures and the respective Bethe-Born factors determined as described in parts I [49] and II [90]. Tables IV–IX summa-

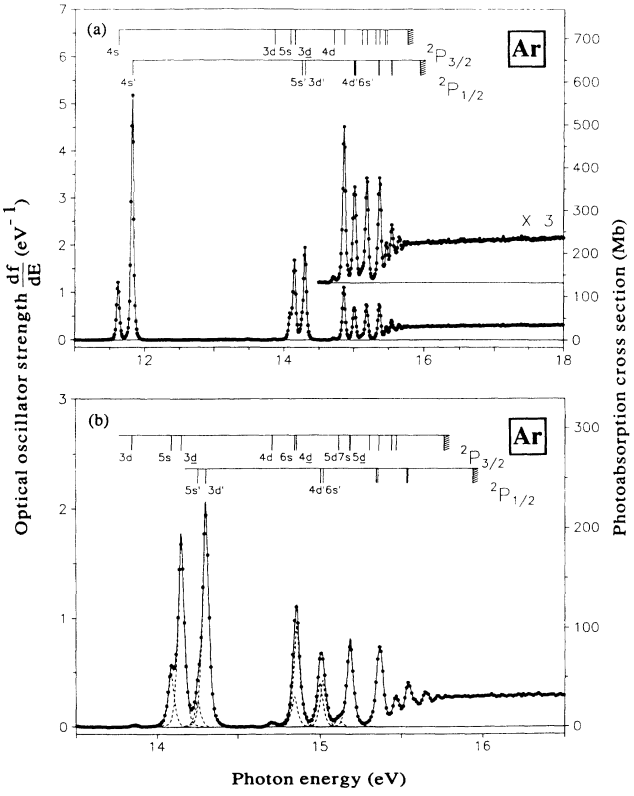

FIG. 9. Absolute oscillator strengths for the photoabsorption of argon obtained using the high-resolution dipole (e,e) spectrometer (FWHM of 0.048 eV). The assignments and energy positions are taken from Ref. [95]. (a) 11–18 eV. (b) Expanded view of the 13.5–16.5 eV energy region. The deconvoluted peaks are shown as dashed lines.

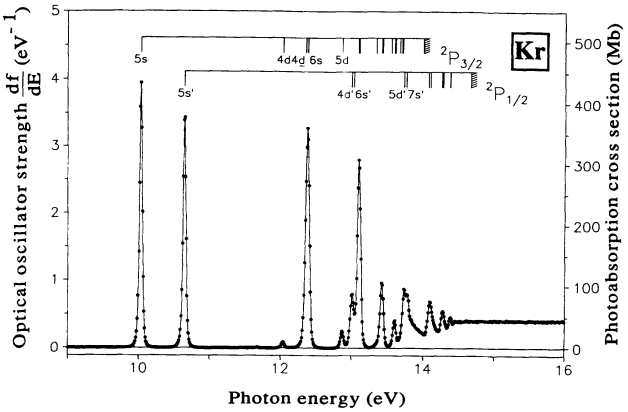

FIG. 10. Absolute oscillator strengths for the photoabsorption of krypton obtained using the high-resolution dipole (e,e) spectrometer (FWHM of 0.048 eV) in the energy region 9–16 eV. The assignments and energy positions are taken from Ref. [95].

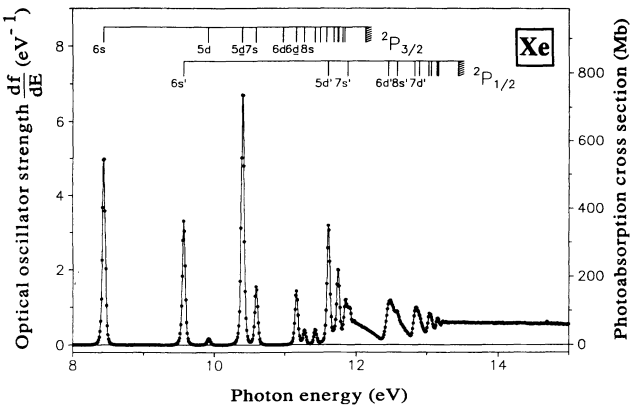

FIG. 12. Absolute oscillator strengths for the photoabsorption of xenon obtained using the high-resolution dipole (e,e) spectrometer (FWHM of 0.048 eV) in the energy region 8–15 eV. The assignments and energy positions are taken from Ref. [95].

rize the optical oscillator strengths for the discrete transitions of the three noble gases obtained from the analyses of the spectra (Figs. 9–13) at the highest resolution (0.048-eV FWHM). The uncertainties are estimated to be $\sim 5\%$ for resolved transitions and $\leq 10\%$ for unresolved peaks such as the $5s$, $5s'$, $3d$, and $3d'$ excited states of argon due to the additional errors involved in deconvoluting the peaks. Other previously reported experimental and theoretical oscillator strengths for the discrete electronic transitions of the three noble gases are also shown

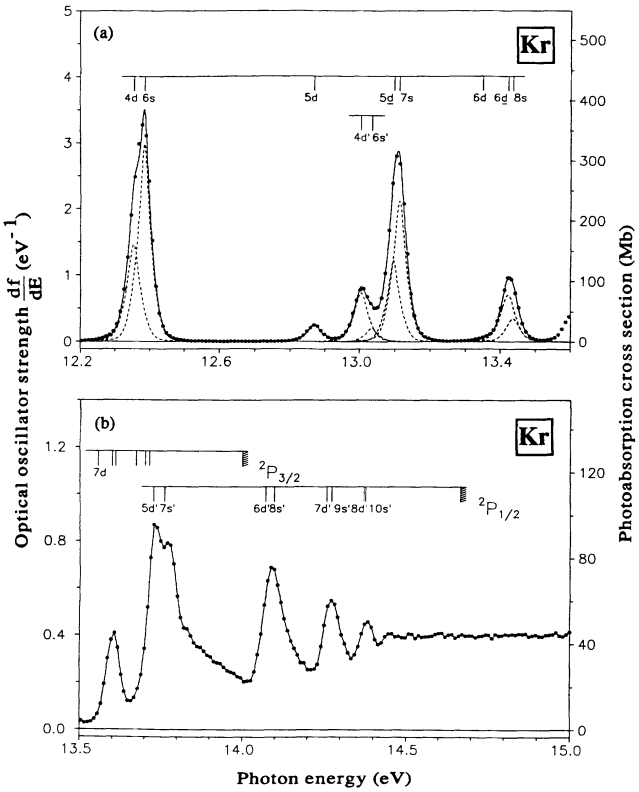

FIG. 11. Absolute oscillator strengths for the photoabsorption of krypton obtained using the high-resolution dipole (e,e) spectrometer (FWHM of 0.048 eV). The assignments and energy positions are taken from Ref. [95]. (a) Expanded view of the 12.2–13.6 eV energy region. The deconvoluted peaks are shown as dashed lines. (b) Expanded view of the 13.5–15.0 eV energy region.

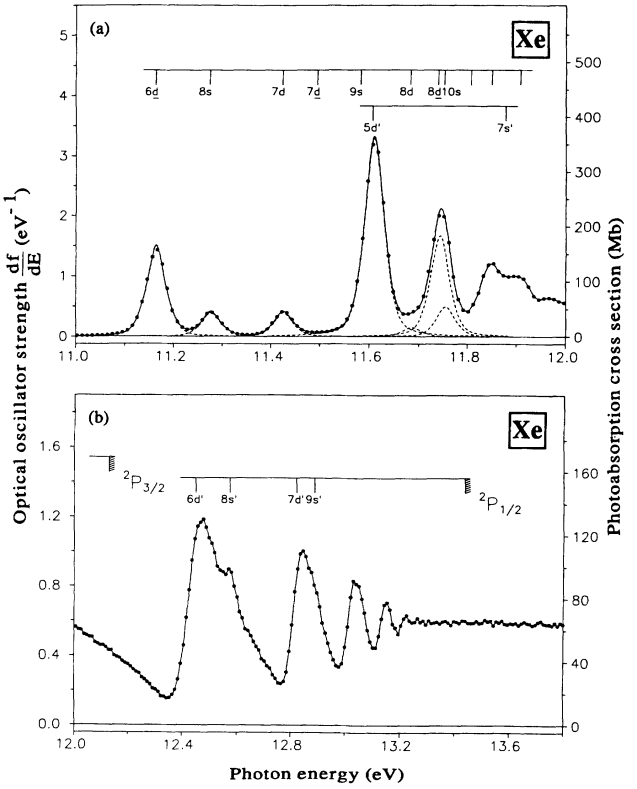

FIG. 13. Absolute oscillator strengths for the photoabsorption of xenon obtained using the high-resolution dipole (e,e) spectrometer (FWHM of 0.048 eV). The assignments and energy positions are taken from Ref. [95]. (a) Expanded view of the 11–12 eV energy region. The deconvoluted peaks are shown as dashed lines. (b) Expanded view of the 12–13.7 eV energy region.

TABLE IV. Theoretical and experimental determinations of the absolute optical oscillator strengths for the $3s^2 3p^6 \rightarrow 3s^2 3p^5 ({}^2P_{3/2,1/2}) 4s$ discrete transitions of argon. Estimated uncertainties in the experimental measurements are shown in parentheses.

	Oscillator strength for transition from $3s^2 3p^6 \rightarrow 3s^2 3p^5 m$ where m is		Oscillator strength ratio
	$({}^2P_{3/2}) 4s$ (a_1) (11.624 eV)[a]	$({}^2P_{1/2}) 4s'$ (a_2) (11.828 eV)	(a_1/a_2)
Theory			
Amus'ya [35]	0.298[b]		
Cooper [1]	0.33[b]		
Stewart [46]		0.270	
Albat, Gruen, and Wirsam [45]	0.048	0.188	0.255
Gruzdev and Loginov [43]	0.061	0.231	0.264
Lee [42]	0.059	0.30	0.197
Lee and Lu [41]	0.080	0.210	0.381
Aymar, Feneuille, and Klapisch [40]			
(a) dipole length	0.071	0.286	0.248
(b) dipole velocity	0.065	0.252	0.258
Gruzdev [38]	0.075	0.15	0.500
Knox [36]			
(a) wave function	0.052	0.170	0.306
(b) semiempirical	0.049	0.200	0.245
Experiment			
Present work [HR dipole (e,e)]	0.0662 (0.0033)	0.265 (0.013)	0.250
Tsurubuchi, Watanabe, and Arikawa [55] (Absolute self-absorption)	0.057 (0.003)	0.213 (0.011)	0.268
Li *et al.* [84] (Electron impact)	0.058 (0.003)	0.222 (0.02)	0.261
Chornay, King, and Buckman [68] (Lifetime: electron-photon coincidence)	0.065 (0.005)		
Westerveld, Malder, and Van Eck [53] (Absolute self-absorption)	0.063 (0.005)	0.240 (0.02)	0.263
Geiger [83] (Electron impact)	0.066	0.255	0.259
Vallee, Ranson and Chapelle [73] (Pressure-broadening profile)	0.051 (0.007)	0.210 (0.030)	0.243
Kuyatt [96] (Electron impact)	0.067	0.267	0.251
Copley and Camm [72] (Pressure-broadening profile)	0.076 (0.008)	0.283 (0.024)	0.269
Irwin, Livingston, and Kernahan [65] (Lifetime: beam foil)	0.083 (0.027)	0.35 (0.130)	0.237
Natali, Kuyatt, and Miekzarek [87] (Electron impact)	0.070	0.278	0.252
McConkey and Donaldson [76] (Electron excitation function)	0.096 (0.02)		
Jongh and Eck [52] (Relative self-absorption)		0.22 (0.02)	
Geiger [79] (Electron impact)	0.047 (0.009)	0.186 (0.037)	0.253
Lawrence [64] (Lifetime: delay coincidence)	0.059 (0.003)	0.228 (0.021)	0.259
Morack and Fairchild [63] (Lifetime: delayed coincidence)	0.024 (0.003)		
Lewis [70] (Pressure-broadening profile)	0.063 (0.004)	0.278 (0.002)	0.227
Chamberlain *et al.* [78] (Electron impact)	0.049	0.181	0.271

[a]The transition energies were obtained from Ref. [95].
[b]Summed oscillator strength $(a_1 + a_2)$.

in the tables for comparison.

Figure 9(a) shows a typical absolute differential optical oscillator strength spectrum of argon obtained at a resolution of 0.048 eV FWHM over the energy range 11–18 eV. Figure 9(b) shows an expanded view of the spectrum in the 13.5–16.5 eV energy region, including the fitted peaks corresponding to partially resolved or unresolved states. Since most of the previously reported experimental [52,53,63,65,68,70,72,73,76,78,79,84] and theoretical [36,38,40,43,45,46] data are restricted mainly to the $4s$ (a_1) and $4s'$ (a_2) resonance lines, the results for these two lines are presented separately in Table IV. The designations a_1,a_2; b_1,b_2; and c_1,c_2 are used for convenience in the present work for the respective resonance ns, ns' lines of argon, krypton, and xenon. Immediately it can be seen that there are great variations in the oscillator strength values reported for the $4s$ and $4s'$ lines in both experiment and also in the theoretical calculations. However, experimental work gives a reasonably consistent result (~ 0.25) for the oscillator strength ratio (a_1/a_2) as shown in the fourth column of Table IV. This suggests that systematic errors, such as uncertainties in measuring the target density or errors in normalizing the data, may be the cause of the large variations in the absolute values. The summed absolute optical oscillator strength (i.e., a_1+a_2) calculated by Cooper [1] using a one-electron approximation agrees very well with the sum of presently measured values (0.331) while the value (0.298) reported by Amus'ya [35] using the RPAE method is slightly lower. The calculated data reported by Aymar, Feneuille, and Klapisch [40] for a_1 and a_2 and the value reported by Stewart [46] for a_2 are consistent with the present work. The calculations by Knox [36] and by Albat, Gruen, and Wirsam [45] give very low values. Ex-

TABLE V. Theoretical and experimental determinations of the absolute optical oscillator strengths for discrete transitions of argon in the energy regions (a) 13.80–14.85 eV and (b) 14.85–15.30 eV. Estimated uncertainties in the experimental measurements are shown in parentheses.

	(a) 13.80–14.85 eV Oscillator strength from $3s^23p^6 \rightarrow 3s^23p^5m$ where m is						
	$(^2P_{3/2})3d$[a] (13.864 eV)[b]	$(^2P_{3/2})5s$ (14.090 eV)	$(^2P_{3/2})3\underline{d}$ (14.153 eV)	$(^2P_{1/2})5s'$ (14.255 eV)	$(^2P_{1/2})3d'$ (14.304 eV)	$(^2P_{3/2})4d$ (14.711 eV)	$(^2P_{3/2})6s$ (14.848 eV)
Theory							
Lee [42]	0.0016	0.045	0.045	0.039	0.128	0.0026	0.023
Lee and Lu [41]	0.0011	0.034	0.053	0.025	0.11	0.0031	0.014
Experiment							
Present work [HR dipole (e,e)]	0.0013 (0.0001)	0.0264 (0.0026)	0.0914 (0.0091)	0.0126 (0.0013)	0.106 (0.011)	0.0019 (0.0002)	0.0144 (0.0014)
Westerveld, Mulder, and Van Eck [53] (Absolute self-absorption)	0.00089 (0.00007)	0.025 (0.002)	0.079 (0.006)	0.0106 (0.0008)	0.086 (0.007)		
Geiger [83] (Electron impact)	<0.0025	0.032	0.108	0.0108	0.097		
Natali, Kuyatt, and Miekzarek [87] (Electron impact)	0.0010	0.028	0.092	0.0124	0.110	0.004	0.0094
Wiese, Smith, and Miles [97][c] (Lifetime data from Ref. [64])		0.0268	0.093	0.0119	0.0106		
Lawrence [64] (Lifetime: delayed coincidence)		0.028 (0.002)	0.093 (0.006)	0.013 (0.003)	0.107 (0.015)		

	(b) 14.85–15.30 eV Oscillator strength from $3s^23p^6 \rightarrow 3s^23p^5m$ where m is						Total
	$(^2P_{3/2})4\underline{d}$[a] (14.859 eV)[b]	$(^2P_{1/2})4d'$ (15.004 eV)	$(^2P_{1/2})6s'$ (15.022 eV)	$(^2P_{3/2})5d$ (15.118 eV)	$(^2P_{3/2})7s$ (15.186 eV)	$(^2P_{3/2})5\underline{d}$ (15.190 eV)	to ionization
Theory							
Lee [42]	0.036						0.82
Lee and Lu [41]	0.039	0.032	0.013				
Experiment							
Present work [HR dipole (e,e)]	0.0484 (0.0048)	0.0209 (0.0021)	0.0221 (0.0022)	0.0041 (0.0004)	0.0426 (0.0043)	0.0426 (0.0043)	0.859 (0.0043)
Natali, Kuyatt, and Miekzarek [87] (Electron impact)	0.048	0.015	0.0224	0.0032	0.0139	0.0234	0.827

[a] nd and $n\underline{d}$ refer to the $nd[1/2]$ and $nd[3/2]$ states, respectively, which converge to the same $^2P_{3/2}$ limit.
[b] The transition energies were obtained from Ref. [95].
[c] Values obtained by reanalyzing the lifetime data of Lawrence [64].

perimentally the oscillator strength values reported by three groups [52,53,55] using the self-absorption method are all lower than the present values by 5–20%. Lifetime measurements performed by Irwin, Livingston, and Kernahan [65] using the beam-foil method show values for a_1 and a_2 much higher than the present work, while the value of a_1 reported by Morack and Fairchild [63], who used a delayed coincidence method, is much lower than all other experimental values. The values measured by Copley and Camm [72] and by Lewis [70] from analysis of the pressure-broadening profiles are consistent with the present work. Several electron-impact-based ex-

TABLE VI. Theoretical and experimental determinations of the absolute optical oscillator strengths for the $4s^24p^6 \rightarrow 4s^24p^5(^2P_{3/2,1/2})5s$ discrete transitions of krypton. Estimated uncertainties in the experimental measurements are shown in parentheses.

	Oscillator strength for transition from $4s^24p^6 \rightarrow 4s^24p^5m$ where m is		Oscillator strength ratio (b_1/b_2)
	$(^2P_{3/2})5s$ (b_1) (10.033 eV)[a]	$(^2P_{1/2})5s'$ (b_2) (10.644 eV)	
	Theory		
Amus'ya [35]	0.353[b]		
Cooper [1]	0.405[b]		
Aymar and Coulombe [47]			
(a) dipole length	0.176	0.177	0.994
(b) dipole velocity	0.193	0.172	1.122
Geiger [82]	0.250	0.143	1.748
Gruzdev and Loginov (1975) [44]	0.190	0.177	1.073
Aymar, Feneuille, and Klapisch [40]			
(a) dipole length	0.215	0.215	1.000
(b) dipole velocity	0.185	0.164	1.128
Gruzdev [38]	0.20	0.20	1.000
Dow and Knox [37]			
(a) wave function	0.138	0.136	1.015
(b) semiempirical	0.152	0.153	0.993
	Experiment		
Present work [HR dipole (e,e)]	0.214 (0.011)	0.193 (0.010)	1.109
Tsurubuchi, Watanabe, and Arikawa [55] (Absolute self-absorption)	0.155 (0.011)	0.139 (0.010)	1.115
Takayanagi *et al.* [85] (Electron impact)	0.143 (0.015)	0.127 (0.015)	1.126
Ferrell, Payne and Garrett [75] (Phase matching)		0.180 (0.027)	
Matthias *et al.* [67] (Lifetime: resonance fluoresonance)	0.208 (0.006)	0.197 (0.006)	1.056
Geiger [82] (Electron impact)	0.195	0.173	1.127
Natali, Kuyatt, and Miekzarek [87] (Electron impact)	0.212	0.191	1.110
Jongh and Eck [52] (Relative self-absorption)		0.142 (0.015)	
Geiger [79] (Electron impact)	0.173 (0.035)	0.173 (0.035)	1.000
Griffin and Hutchson [58] (Total absorption)	0.187 (0.006)	0.193 (0.009)	0.969
Chashchina and Shrieder [59] (Linear absorption)	0.21 (0.05)	0.21 (0.05)	1.000
Lewis [70] (Pressure-broadening profile)	0.204 (0.02)	0.184 (0.02)	1.109
Wilkinson [56] (Total absorption)	0.159	0.135	1.178
Turner [62] (Lifetime: resonance imprisonment)	0.166		

[a]The transition energies were obtained from Ref. [95].
[b]Summed oscillator strength (b_1+b_2).

TABLE VII. Theoretical and experimental determinations of the absolute optical oscillator strengths for discrete transitions of krypton in the energy regions (a) 11.90–13.05 and (b) 13.05–13.50 eV. Estimated uncertainties in the experimental measurements are shown in parentheses.

	(a) 11.90–13.05 eV Oscillator strength from $4s^24p^6 \rightarrow 4s^24p^5m$ where m is					
	$(^2P_{3/2})4d$[a] (12.037 eV)[b]	$(^2P_{3/2})4\underline{d}$ (12.355 eV)	$(^2P_{3/2})6s$ (12.385 eV)	$(^2P_{3/2})5d$ (12.870 eV)	$(^2P_{1/2})4d'$ (13.005 eV)	$(^2P_{1/2})6s'$ (13.037 eV)
			Theory			
Geiger [82]	0.0144	0.0973	0.108	0.0114	0.0438	0.0065
			Experiment			
Present work [HR dipole (e,e)]	0.0053 (0.0003)	0.0824 (0.0082)	0.154 (0.015)	0.0140 (0.0014)	0.0435 (0.0044)	0.0105 (0.0011)
Geiger [82] (Electron impact)	0.0055	0.0649	0.142	0.014	0.0439	0.015
Natali, Kuyatt, and Miekzarek [87] (Electron impact)	0.0044	0.0817	0.152	0.0138	0.0420	0.0056

	(b) 13.05–13.50 eV Oscillator strength from $4s^24p^6 \rightarrow 4s^24p^5m$ where m is					Total to ionization
	$(^2P_{3/2})5\underline{d}$[a] (13.099 eV)[b]	$(^2P_{3/2})7s$ (13.114 eV)	$(^2P_{3/2})6d$ (13.350 eV)	$(^2P_{3/2})6\underline{d}$ (13.423 eV)	$(^2P_{3/2})8s$ (13.437 eV)	
			Theory			
Geiger [82]	0.0960	0.0436	0.0025	0.0307	0.0163	
			Experiment			
Present work [HR dipole (e,e)]	0.0610 (0.0061)	0.113 (0.011)	0.0015 (0.0002)	0.0439 (0.0044)	0.0203 (0.0020)	1.126 (0.056)
Geiger [82] (Electron impact)	0.187	0.187	0.0042	0.054	0.054	
Natali, Kuyatt, and Miekzarek [87] (Electron impact)	0.119	0.048	0.0024	0.0295	0.0290	1.10

[a] nd and $n\underline{d}$ refer to the $nd[1/2]$ and $nd[3/2]$ states, respectively, which converge to the same $^2P_{3/2}$ limit.
[b] The transition energies were obtained from Ref. [95].

perimental methods have been employed for deriving the absolute oscillator strengths for a_1 and a_2. The values reported by Chamberlain *et al.* [78], Geiger in his earlier work [79], and Li *et al.* [84] are all lower than those measured in the present work. However, the unpublished data of Natali, Kuyatt, and Miekzarek [87], the data of Kuyatt [96] which are quoted in the compilation of Eggarter [89], and the later work of Geiger [83] which has been quoted in Refs. [53,88] show quite good agreement with the presently measured values. In a compilation published by Wiese, Smith, and Miles [97] values of a_1 and a_2 (not shown in Table IV) were obtained from averaging the data reported by Lawrence [64] and Lewis [70].

A summary of the absolute optical oscillator strengths for the discrete transitions of argon at higher energies is given in Tables V(a) and V(b). Two sets of theoretical results [41,42] have been published, but both show substantial differences with the presently reported and most other experimental data. The lifetime measurements of Lawrence [64] obtained using a pulsed electron source show good agreement with the present values for $5s$, $3\underline{d}$, $5s'$, and $3d'$ transition lines. A reanalysis of the lifetime data of Lawrence [64] by Wiese, Smith, and Miles [97] gave absolute oscillator strength values for the above four transition lines which are also consistent with the present work. Similar to the situation for the $4s$ and $4s'$ resonance lines the self-absorption data for other lines at higher energies measured by Westerveld, Mulder, and Van Eck [53] are lower than the present values. A more comprehensive data set was reported in the electron-impact-based work of Natali, Kuyatt, and Miekzarek [87] and the oscillator strength values for most of the more intense lines are consistent with the present work. The total discrete oscillator strength sum up to the $^2P_{3/2}$ ionization threshold of argon has been determined in the present work to be 0.859, a value which agrees within 5% with estimates of 0.82 calculated by Lee [42] and 0.827 measured by Natali, Kuyatt, and Miekzarek [87]. In the earlier compilation reported by Eggarter [89] the total discrete oscillator strength of argon was estimated to be 0.793 on the basis of the more limited data available at that time.

Figure 10 shows the presently determined absolute differential optical oscillator strength spectrum for krypton over the energy range 9–16 eV. Figures 11(a) and 11(b) show expanded views of the spectrum in the energy regions 12.2–13.6 and 13.5–15 eV, respectively. Since higher members of the ns' and nd' series which converge to the $^2P_{1/2}$ ionization threshold are above the $^2P_{3/2}$ ion-

ization threshold, autoionizing resonance profiles are observed as shown in Fig. 11(b) due to the interaction between the discrete and continuum states. The absolute optical oscillator strengths for the individual discrete electronic transitions of krypton determined in the present work are summarized in Tables VI and VII. There are considerable variations between the various experimental and theoretical oscillator strength values for both the $5s$ (b_1) and the $5s'$ (b_2) resonance lines as can be seen in Table VI. However, on the basis of the oscillator strength ratio (b_1/b_2) the reported data can be divided into two groups. For one group the ratio is close to 1 while for the other it is ~ 1.1. The summed absolute optical oscillator strength (i.e., 0.405 for b_1+b_2) computed by Cooper [1] is consistent with the present value (0.407). The values of b_1 and b_2 calculated by Dow and Knox [37] are too low compared with the present and most other experimental work. Similar to the situation for argon

TABLE VIII. Theoretical and experimental determinations of the absolute optical oscillator strengths for the $5s^25p^6 \rightarrow 5s^25p^5(^2P_{3/2,1/2})6s$ discrete transitions of xenon. Estimated uncertainties in the experimental measurements are shown in parentheses.

	Oscillator strength for transition from $5s^25p^6 \rightarrow 5s^25p^5m$ where m is		Oscillator strength ratio
	$(^2P_{3/2})6s$ (c_1) (8.437 eV)[a]	$(^2P_{1/2})6s'$ (c_2) (9.570 eV)	(c_1/c_2)
	Theory		
Amus'ya [35]	0.403[b]		
Aymar and Coulombe [47]			
(a) dipole length	0.282	0.306	0.922
(b) dipole velocity	0.294	0.270	1.089
Geiger [82]	0.28	0.365	0.767
Aymar, Feneuille, and Kapisch [40]			
(a) dipole length	0.273	0.235	1.162
(b) dipole velocity	0.176	0.118	1.492
Kim *et al.* [39]	0.212	0.189	1.122
Gruzdev [38]	0.28	0.25	1.120
Dow and Knox [37]			
(a) wave function	0.194	0.147	1.320
(b) semiempirical	0.190	0.170	1.118
	Experiment		
Present work [HR dipole (e,e)]	0.273 (0.014)	0.186 (0.009)	1.468
Suzuki *et al.* [86] (Electron impact)	0.222 (0.027)	0.158 (0.019)	1.405
Ferrell, Payne, and Garrett [75] (Phase matching)	0.260 (0.05)	0.19 (0.04)	1.368
Matthias *et al.* [67] (Lifetime: resonance fluorescence)	0.263 (0.007)	0.229 (0.007)	1.148
Geiger [82] (Electron impact)	0.26	0.19	1.368
Delage and Carette [81] (Electron impact)	0.183	0.169	1.083
Natali, Kuyatt, and Miekzarek [87] (Electron impact)	0.272	0.189	1.439
Wieme and Mortier [66] (Lifetime: resonance imprisonment)	0.213 (0.020)	0.180 (0.040)	1.183
Geiger [79] (Electron impact)	0.26	0.19	1.368
Griffin and Hutchson [58] (Total absorption)		0.194 (0.005)	
Lewis [70] (Pressure-broadening profile)	0.256 (0.008)	0.238 (0.015)	1.071
Wilkinson [57] (Total absorption)	0.260 (0.020)	0.270 (0.020)	0.963
Anderson [61] (Lifetime: level crossing)	0.256 (0.008)	0.238 (0.015)	1.076

[a]The transition energies were obtained from Ref. [95].
[b]Summed oscillator strength (c_1+c_2).

the self-absorption data reported by Tsurubuchi, Watanabe, and Arikawa [55] for b_1 and b_2 and Jongh and Eck [52] for b_2 are lower than the presently reported values. The experimental data of Ferrell, Payne, and Garrett [75] using the phase-matching method, that of Matthias *et al.* [67], which was obtained by measuring the lifetimes of the radiative fluorescence, the data of Natali, Kuyatt, and Miekzarek [87], who applied the electron-impact-based method, and the data of Lewis [70], which were obtained by studying the pressure-broadening profiles, are all in good agreement with the presently reported oscillator strength values for b_1 and b_2. The absolute optical oscillator strength values for transitions at higher energies are shown in Tables VII(a) and VII(b). The theoretical data available are limited to the semiempirical calculations reported by Geiger [82]. Only the value for the $4d'$ resonance line computed by Geiger [82] agrees with the present results. Previously published data obtained by the application of electron-impact-based methods [82,87] together with the present dipole (e,e) work provide the only available optical oscillator strength data for the discrete transitions of krypton at higher energies. Generally quite good agreement for the absolute optical oscillator strength values is observed among the different electron-impact methods for most of the transition lines. The total discrete oscillator strength up to the $^2P_{3/2}$ ionization threshold is determined to be 1.126 in the present work compared with an estimate of 1.10 reported by Natali, Kuyatt, and Miekzarek [87].

Figure 12 shows the high-resolution absolute differential oscillator strength spectrum of xenon obtained in the present work over the energy region 8–15

TABLE IX. Theoretical and experimental determinations of the absolute optical oscillator strengths for discrete transitions of xenon in the energy regions (a) 9.80–11.45 eV and (b) 11.45–11.80 eV. Estimated uncertainties in the experimental measurements are shown in parentheses.

	(a) 9.80–11.45 eV Oscillator strength from $5s^25p^6 \rightarrow 5s^25p^5m$ where m is						
	$(^2P_{3/2})5d$[a] (9.917 eV)[b]	$(^2P_{3/2})5\underline{d}$ (10.401 eV)	$(^2P_{3/2})7s$ (10.593 eV)	$(^2P_{3/2}6d$ (10.979 eV)	$(^2P_{1/2})6\underline{d}$ (11.163 eV)	$(^2P_{3/2})8s$ (11.274 eV)	$(^2P_{3/2})7d$ (11.423 eV)
			Theory				
Geiger [82]	0.0237	0.550	0.0769	0.0025	0.0940	0.0126	0.0190
			Experiment				
Present work [HR dipole (e,e)]	0.0105 (0.0005)	0.379 (0.019)	0.0859 (0.0043)	<0.001	0.0835 (0.0084)	0.0222 (0.0022)	0.0227 (0.0023)
Ferrell, Payne, and Garrett [75] (Phase matching)		0.370 (0.07)	0.088 (0.01)				
Kramer, Chen, and Payne [74] (Phase matching)			0.098				
Geiger [82] (Electron impact)	0.0095	0.395	0.0968	0.0025	0.0862	0.0236	0.0217
Delage and Carette [81] (Electron impact)	0.019	0.395[c]	0.110		0.123	0.032	0.027
Natali, Kuyatt, and Miekzarek [87] (Electron impact)	0.012	0.381	0.09	0.002	0.082	0.021	0.021

	(b) 11.45–11.80 eV Oscillator strength from $5s^25p^6 \rightarrow 5s^25p^5m$ where m is						Total
	$(^2P_{3/2})7\underline{d}$[a] (11.495 eV)[b]	$(^2P_{3/2})9s$ (11.583 eV)	$(^2P_{1/2})5d'$ (11.607 eV)	$(^2P_{3/2})8d$ (11.683 eV)	$(^2P_{3/2})8\underline{d}$ (11.740 eV)	$(^2P_{3/2})10s$ (11.752 eV)	to ionization
			Theory				
Geiger [82]	0.0024	0.0009	0.206	0.0155	0.123	0.0169	
			Experiment				
Present work [HR dipole (e,e)]	<0.001	<0.001	0.191 (0.019)	0.0088 (0.0009)	0.0967 (0.0097)	0.0288 (0.0029)	1.606 (0.080)
Geiger [82] (Electron impact)	0.004	0.006	0.205	0.0096	0.123	0.0204	1.640[d]
Delage and Carette [81] (Electron impact)		0.251	0.251	0.171	0.171	0.171	
Natali, Kuyatt, and Garrett [87] (Electron impact)	0.0003	0.001	0.186	0.006	0.109	0.015	

[a] nd and $n\underline{d}$ refer to the $nd[1/2]$ and $nd[3/2]$ states, respectively, which converge to the same $^2P_{3/2}$ limit.
[b] The transition energies were obtained from Ref. [95].
[c] This value was normalized to the experimental value of Geiger [82].
[d] This value is quoted in Ref. [88].

eV. Figures 13(a) and 13(b) show expanded views of the spectrum in the energy regions 11–12 and 12–13.7 eV, respectively. Broad autoionizing resonance profiles of higher members of the ns' and nd' series above the $^2P_{3/2}$ limit are observed as can be seen in Fig. 13(b). Tables VIII and IX summarize all the discrete absolute optical oscillator strengths values for xenon determined in the present work along with various previously reported theoretical and experimental data. It can be seen from Table VIII that there are large variations in the oscillator strengths reported for the $6s$ (c_1) and $6s'$ (c_2) resonance lines. The oscillator strength ratio c_1/c_2 also shows considerable variation from 0.767–1.492 for theory and 0.963–1.468 for experiment. Some theoretical data show agreement of either c_1 [38,40,47,82] or c_2 [39] with the present work. However, no single set of theoretical data are consistent with the present work for both c_1 and c_2 values. Experimentally, the phase-matching data of Ferrell, Payne, and Garrett [75], and the electron-impact data of Geiger [79,82] and Natali, Kuyatt, and Miekzarek [87] show good agreement with the presently reported c_1 and c_2 values. The recently reported data of Suzuki *et al.* [86] are ~20% lower than the present values. Similar discrepancies were observed in the cases of the a_1 and a_2 transitions of argon and the b_1 and b_2 transitions of krypton between the present work and absolute oscillator strengths reported by the same group [84,85] (see above). The absolute data for the discrete transitions at higher energies are shown in Tables IX(a) and IX(b). The phase-matching data of Ferrell, Payne, and Garrett [75] show excellent agreement for the $5\underline{d}$ and $7s$ lines with the present values while the earlier phase-matching value reported by Kramer, Chen, and Payne [74] for the $7s$ line is slightly higher. Other more comprehensive data for the discrete transitions of xenon at higher energies have all been measured by electron-impact-based methods [81,82,87]. It can be seen that the oscillator strengths determined in the present work are in excellent agreement over the whole energy range with the data reported by Natali, Kuyatt, and Miekzarek [87] except for the $10s$ line. This discrepancy may be caused by errors in deconvoluting the peak. The data of Geiger [82] are consistent with the present work for most of the transitions while the data of Delage and Carette [81], which have been normalized on the $5\underline{d}$ line from the data of Geiger [82], show considerable variations compared with the presently reported values. Finally, the total oscillator strength sum up to the $^2P_{3/2}$ ionization threshold of xenon was determined to be 1.606 in the present work, which is in good agreement with the estimate of 1.640 reported by Geiger [82].

C. High-resolution measurements of the photoabsorption oscillator strengths in the autoionizing resonance regions due to the excitation of the inner-valence *s* electrons

The profiles and relative cross sections of the autoionizing excited-state resonances of argon, krypton, and xenon involving the excitation of an inner-valence ms electron have been previously studied in some detail experimentally [19,23,93,98–104]. Although double-excitation processes have also been reported in these energy regions [93,99–101] these transitions are extremely weak and they are not specifically identified in the present work. Absolute intensity measurements [19,23,98,104] have also been reported. In the present study Bethe-Born converted electron-energy-loss spectra of the three noble gases were obtained in these regions with the use of the high-resolution dipole (e,e) spectrometer at a resolution of 0.048-eV FWHM. The resulting relative optical oscillator strength spectra were then normalized in the respective smooth continua at 21.218 eV for argon and krypton, and at 16.848 eV for xenon using the absolute data determined by Samson and Yin [28].

Figure 14 shows the resulting absolute optical oscillator strength spectrum of argon in the energy region 25–30 eV. The absolute data reported by Carlson *et al.* [23] (crosses) using synchrotron radiation and Samson [19,98] (open circles) employing a double-ionization chamber are also shown in Fig. 14. Only the assignments for the transitions involving the excitation of a $3s$ electron to np states are shown. The energy positions of the resonances as indicated in the manifold on Fig. 14 are taken from the high-resolution photoabsorption data reported by Madden, Ederer, and Codling [93]. The data of Carlson *et al.* [23] show a slight shift in energy scale with respect to the present work, which may be due to errors in digitizing the data from the small figure in the original paper. The absolute data reported by Samson [19,98] and Carlson *et al.* [23] are in good agreement with the present work in the energy region 25–26 eV. However, the Samson data are higher than the present work above 29 eV while the data of Carlson *et al.* [23] are lower. It seems likely that line-saturation effects, which have been discussed in detail in Refs. [48–51], are observed in the direct optical data reported by Samson [19,98] for the $3s \rightarrow np$ transitions. As the widths of the $3s \rightarrow np$ transition peaks get much narrower as n increases, line-saturation effects are expected to be more

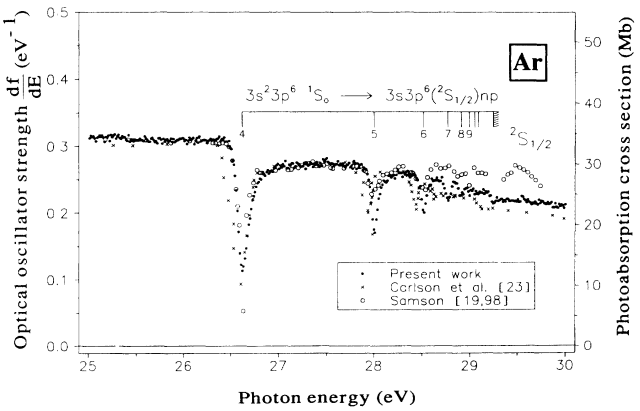

FIG. 14. Absolute oscillator strengths for the photoabsorption of argon in the autoionizing resonance region 25–30 eV. The solid circles represent the present work (FWHM of 0.048 eV) and the open circles and crosses represent the photoionization data reported by Samson [19,98] and Carlson *et al.* [23], respectively. The assignments and energy positions are taken from Ref. [93].

severe for the peaks at higher n values. It can be seen from Fig. 14 that for the relatively broad $3s \rightarrow 4p$ transition, the data of Samson [19,98] show a lower minimum consistent with the higher experimental resolution than that used in the present work. However, for the narrower $3s \rightarrow 5p$ transition the present work (which cannot show line-saturation effects) gives a lower minimum than the Samson data [19,98]. This observation strongly suggests the presence of line-saturation effects at larger n due to the finite bandwidth of the optical experiments [19,98]. The same phenomenon is observed for the transitions to the higher np states.

Figure 15 shows the presently determined high-resolution absolute optical oscillator strength spectrum of krypton in the energy region 23–28.5 eV along with the reported absolute data of Samson [19,98]. The assignments and energy positions for the $4s \rightarrow np$ transitions are taken from Codling and Madden [99,101]. There are two $J=1$ components for the transition $4s^2 4p^6\,{}^1S_0 \rightarrow 4s4p^6({}^2S_{1/2})np$ where one Rydberg series is labeled as n and the other one is labeled as $\underline{n}$ as shown in Fig. 15. Only $\underline{n}=\underline{5}$ and $\underline{6}$ for the latter series are unambiguously assigned [99–101]. The line-saturation effects that are observed in the optical data reported by Samson [19,98] for argon are also seen in the corresponding direct optical data for krypton. The effect is especially severe for the $4s \rightarrow 7p$ transition. Samson [19,98] and other workers using direct optical methods [99–101,104] have reported a peak (Q) at 24.735 eV which was not observed in the present work.

The presently determined high-resolution absolute optical oscillator strength spectrum of xenon in the energy region 20–24 eV is shown in Fig. 16. The figure also shows the photoionization cross sections for xenon in this energy range reported by Samson [19], which are significantly lower than those determined in the present work. The assignments and energy positions for the $5s \rightarrow np$ transitions are taken from the data reported by Codling and Madden [99,101]. Only one Rydberg series

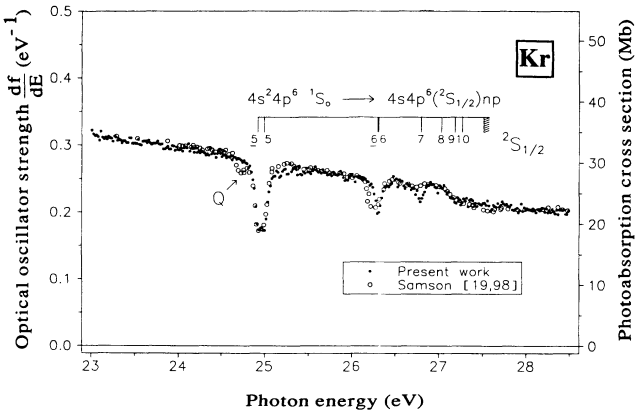

FIG. 15. Absolute oscillator strengths for the photoabsorption of krypton in the autoionizing resonance region 23–28.5 eV. The solid circles represent the present work (FWHM of 0.048 eV) and the open circles represent the photoionization data reported by Samson [19,98]. The assignments and energy positions are taken from Refs. [99,101].

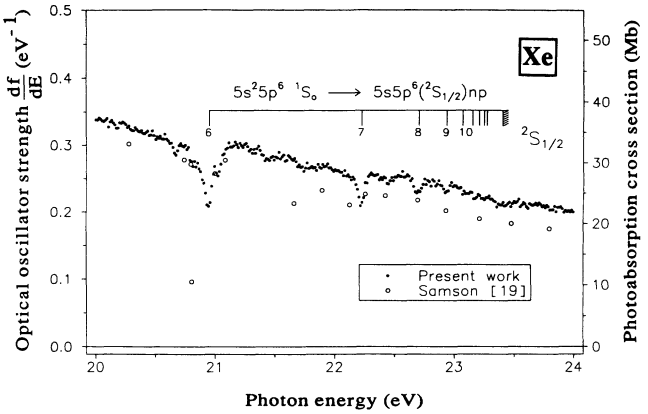

FIG. 16. Absolute oscillator strengths for the photoabsorption of krypton in the autoionizing resonance region 20–24 eV. The solid circles represent the present work (FWHM of 0.048 eV) and the open circles represent the photoionization data reported by Samson [19]. The assignments and energy positions are taken from Refs. [99,101].

of the two $J=1$ components of the $5s \rightarrow np$ transitions converging to the $^2S_{1/2}$ ionization threshold was assigned [99–101].

IV. CONCLUSIONS

Comprehensive absolute differential optical oscillator strength data from experiments on argon, krypton, and xenon in both the discrete and continuum regions have been reported, including measurements at high resolution. The present work represents the completion of the measurements for the noble-gas series using the high-resolution dipole (e,e) method recently developed for measuring absolute optical oscillator strengths for a wide range of transitions in atoms and molecules. The TRK sum-rule normalization method which was used for helium and neon could not be used for argon, krypton, and xenon due to the smaller energy separations between the different subshells of the atoms. Therefore, single-point normalization on very accurate photoabsorption measurements has been used. The presently reported results are compared with theory and also other earlier reported experimental data. In the continuum region the various experimental values generally show reasonable agreement at low energy while there are certain variations at high energy. With the inclusion of more electron correlations and more sophisticated calculations, the theoretical data are in better agreement with experimental values. In the discrete region a wide spread of values is seen for the resonance-line oscillator strengths a_1 and a_2 of argon, b_1 and b_2 of krypton, and c_1 and c_2 of xenon in both experiment and theory. For discrete transitions at higher energies there is a shortage of theoretical data. Electron-impact-based methods have thus far provided most of the absolute optical oscillator strength data for the valence-shell discrete spectra. Generally the present measurements are in quite good agreement with the earlier unpublished electron-impact-based data of Natali, Kuyatt, and Miekzarek [87], which were obtained at lower impact energy. Absolute optical oscillator strengths for the au-

toionizing excited-state regions involving mainly the inner-valence s electrons of the three noble gases have also been obtained. The previously published photoionization data of Samson [19,98] in this energy range show evidence of substantial line-saturation effects.

ACKNOWLEDGMENTS

Financial support for this project was provided by the Natural Sciences and Engineering Research Council of Canada (NSERC) and the Canadian National Networks of Centres of Excellence Programme (Centres of Excellence in Molecular and Interfacial Dynamics). Two of us (W.F.C. and G.R.B.) gratefully acknowledge support from the University of British Columbia and NSERC, respectively. Financial support from The World Laboratory (Lausanne) is acknowledged by X. Guo. We wish to thank Professor J. A. R. Samson for sending us his measured data and for helpful comments on the present work.

*Permanent address: University of Science and Technology of China, Hefei, People's Republic of China.

[1] J. W. Cooper, Phys. Rev. **128**, 681 (1962).
[2] E. J. McGuire, Phys. Rev. **175**, 20 (1968).
[3] M. Ya. Amus'ya, N. A. Cherepkov, and L. V. Chernysheva, Zh. Eksp. Teor. Fiz. **60**, 160 (1971) [Sov. Phys. JETP **33**, 90 (1971)].
[4] D. J. Kennedy and S. T. Manson, Phys. Rev. A **5**, 227 (1972).
[5] P. G. Burke and K. T. Taylor, J. Phys. B **8**, 2620 (1975).
[6] A. Zangwill and P. Soven, Phys. Rev. A **21**, 1561 (1980).
[7] W. R. Johnson and K. T. Cheng, Phys. Rev. A **20**, 978 (1979).
[8] F. A. Parpia, W. R. Johnson, and V. Radojevic, Phys. Rev. A **29**, 3173 (1984).
[9] A. F. Starace, Phys. Rev. A **2**, 118 (1970).
[10] S. T. Manson and J. W. Cooper, Phys. Rev. **165**, 126 (1968).
[11] B. F. Rozsnyai, Phys. Rev. A **42**, 286 (1990).
[12] P. Lee and G. L. Weissler, Phys. Rev. **99**, 540 (1955).
[13] R. E. Huffman, Y. Tanaka, and J. C. Larrabee, J. Chem. Phys. **39**, 902 (1963).
[14] A. P. Lukirskii and T. M. Zimkina, Bull. Acad. Sci. USSR, Phys. Ser. **27**, 808 (1963).
[15] A. P. Lukirskii, I. A. Brytov, and T. M. Zimkina, Opt. Spectrosc. **17**, 234 (1964).
[16] O. P. Rustgi, J. Opt. Soc. Am. **54**, 464 (1964).
[17] D. L. Ederer, Phys. Rev. Lett. **13**, 760 (1964).
[18] P. H. Metzger and G. R. Cook, J. Opt. Soc. Am. **55**, 516 (1965).
[19] J. A. R. Samson, Adv. At. Mol. Phys. **2**, 177 (1966).
[20] R. Haensel, G. Keitel, and P. Schreider, Phys. Rev. **188**, 1375 (1969).
[21] D. R. Denne, J. Phys. D **3**, 1392 (1970).
[22] W. S. Watson, J. Phys. B **5**, 2292 (1972).
[23] R. W. Carlson, D. L. Judge, M. Ogawa, and L. C. Lee, Appl. Opt. **12**, 409 (1973).
[24] J. Lang and W. S. Watson, J. Phys. B **8**, L339 (1975).
[25] J. B. West and G. V. Marr, Proc. R. Soc. London Ser. A **349**, 397 (1976).
[26] G. V. Marr and J. B. West, At. Data Nucl. Data Tables **18**, 497 (1976).
[27] J. B. West and J. Morton, At. Data Nucl. Data Tables **22**, 103 (1978).
[28] J. A. R. Samson and L. Yin, J. Opt. Soc. Am. B **6**, 2326 (1989).
[29] J. A. R. Samson, L. Yin, G. N. Haddad, and G. C. Angel, J. Phys. (Paris) Colloq. IV, Suppl. II. **1**, C1-99 (1991).
[30] M. H. Hecht and I. Lindau, J. Electron Spectrosc. Relat. Phenom. **35**, 211 (1985).
[31] D. M. P. Holland, M. A. MacDonald, and M. A. Hayer, Chem. Phys. **142**, 291 (1990).
[32] N. Saito, I. Suzuki, H. Onuki, and M. Nishi, Rev. Sci. Instrum. **60**, 2190 (1989).
[33] M. J. Van der Wiel and G. Wiebes, Physica **53**, 225 (1971).
[34] Th. M. El-Sherbini and M. J. Van der Wiel, Physica **62**, 119 (1972).
[35] M. Ya. Amus'ya, *Atomic Photoeffect* (Plenum, New York, 1990), p. 170.
[36] R. S. Knox, Phys. Rev. **110**, 375 (1958).
[37] J. D. Dow and R. S. Knox, Phys. Rev. **152**, 50 (1966).
[38] P. F. Gruzdev, Opt. Spectrosc. **22**, 170 (1967).
[39] Y. K. Kim, M. Inokuti, G. E. Chamberlain, and S. R. Mielczarek, Phys. Rev. Lett. **21**, 1146 (1968).
[40] M. Aymar, S. Feneuille, and M. Klapisch, Nucl. Instrum. Methods **90**, 137 (1970).
[41] C. M. Lee and K. T. Lu, Phys. Rev. A **8**, 1241 (1973).
[42] C. M. Lee, Phys. Rev. A **10**, 584 (1974).
[43] P. F. Gruzdev and A. V. Loginov, Opt. Spektrosk. **38**, 411 (1975) [Opt. Spectrosc. **38**, 234 (1975)].
[44] P. F. Gruzdev and A. V. Loginov, Opt. Spektrosk. **38**, 1065 (1975) [Opt. Spectrosc. **38**, 611 (1975)].
[45] R. Albat, N. Gruen, and B. Wirsam, J. Phys. B **8**, L82 (1975).
[46] R. F. Stewart, Mol. Phys. **30**, 745 (1975).
[47] M. Aymar and M. Coulombe, At. Data Nucl. Data Tables **21**, 537 (1978).
[48] W. F. Chan, G. Cooper, K. H. Sze, and C. E. Brion, J. Phys. B **23**, L523 (1990).
[49] W. F. Chan, G. Cooper, and C. E. Brion, Phys. Rev. A **44**, 186 (1991).
[50] R. D. Hudson, Rev. Geophys. Space Phys. **6**, 305 (1971).
[51] S. Brodersen, J. Opt. Soc. Am. **44**, 22 (1954).
[52] J. P. De Jongh and J. Van Eck, Physica **51**, 104 (1971).
[53] W. B. Westerveld, Th. F. A. Mulder, and J. Van Eck, J. Quant. Spectrosc. Radiat. Transfer **21**, 533 (1979).
[54] S. Tsurubuchi, K. Watanabe, and T. Arikawa, J. Phys. B **22**, 2969 (1989).
[55] S. Tsurubuchi, K. Watanabe, and T. Arikawa, J. Phys. Soc. Jpn. **59**, 497 (1990).
[56] P. G. Wilkinson, J. Quant. Spectrosc. Radiat. Transfer **5**, 503 (1965).
[57] P. G. Wilkinson, J. Quant. Spectrosc. Radiat. Transfer **6**, 823 (1966).
[58] P. M. Griffin and J. W. Hutchson, J. Opt. Soc. Am. **59**, 1607 (1969).
[59] G. I. Chashchina and E. Ya. Shreider, Opt. Spectrosc. **22**, 284 (1967).
[60] G. I. Chashchina and E. Ya. Shreider, Opt. Spectrosc. **27**, 79 (1969).

[61] D. K. Anderson, Phys. Rev. **137**, A21 (1965).
[62] R. Turner, Phys. Rev. **140**, A426 (1965).
[63] J. L. Morack and C. E. Fairchild, Phys. Rev. **163**, 125 (1967).
[64] G. M. Lawrence, Phys. Rev. **175**, 40 (1968).
[65] D. Irwin, A. E. Livingston, and J. A. Kernahan, Nucl. Instrum. Methods **110**, 111 (1973).
[66] W. Wieme and P. Mortier, Physica **65**, 198 (1973).
[67] E. Matthias, R. A. Rosenberg, E., D. Poliakoff, M. G. White, S. T. Lee, and D. A. Shirley, Chem. Phys. Lett. **52**, 239 (1977).
[68] D. J. Chornay, G. C. King, and S. J. Buckman, J. Phys. B **17**, 3173 (1984).
[69] D. N. Stacey and J. M. Vaughan, Phys. Lett. **11**, 105 (1964).
[70] E. L. Lewis, Proc. Phys. Soc. **92**, 817 (1967).
[71] J. M. Vaughan, Phys. Rev. **166**, 13 (1968).
[72] G. H. Copley and D. M. Camm, J. Quant. Spectrosc. Radiat. Transfer **14**, 899 (1974).
[73] O. Vallee, P. Ranson, and J. Chapelle, J. Quant. Spectrosc. Radiat. Transfer **18**, 327 (1977).
[74] S. D. Kramer, C. H. Chen, and M. G. Payne, Opt. Lett. **9**, 347 (1984).
[75] W. R. Ferrell, M. G. Payne, and W. R. Garrett, Phys. Rev. A **35**, 5020 (1987).
[76] J. W. McConkey and F. G. Donaldson, Can. J. Phys. **51**, 914 (1973).
[77] J. Geiger, Z. Phys. **177**, 138 (1964).
[78] G. E. Chamberlain, J. G. M. Heideman, J. A. Simpson, and C. E. Kuyatt, in *Abstracts in Proceedings of the Fourth International Conference on the Physics of Electronic and Atomic Collisions, Quebec, 1965,* edited by L. Kerwin and W. Fite (Science Bookcrafters, Hastings-on-Hudson, 1968).
[79] J. Geiger, Phys. Lett. **33A**, 351 (1970).
[80] J. Geiger, in *Proceedings of the Fourth International Conference on Vacuum Ultraviolet Radiation Physics* (Pergamon, New York, 1974), p. 28.
[81] A. Delage and J. D. Carette, Phys. Rev. A **14**, 1345 (1976).
[82] J. Geiger, Z. Phys. A **282**, 129 (1977).
[83] J. Geiger, unpublished observations as quoted in Refs. [53,88].
[84] G. P. Li, T. Takayanagi, K. Wakiya, H. Suzuki, T. Ajiro, S. Yagi, S. S. Kano, and H. Takuma, Phys. Rev. A **38**, 1240 (1988).
[85] T. Takayanagi, G. P. Li, K. Wakiya, H. Suzuki, T. Ajiro, T. Inaba, S. S. Kano, and H. Takuma, Phys. Rev. A **41**, 5948 (1990).
[86] T. Y. Suzuki, Y. Sakai, B. S. Min, T. Takayanagi, K. Wakiya, H. Suzuki, T. Inaba, and H. Takuma, Phys. Rev. A **43**, 5867 (1991).
[87] S. Natali, C. E. Kuyatt, and S. R. Miekzarek, unpublished observations as quoted in Refs. [53,83,88].
[88] J. Berkowitz, *Photoabsorption, Photoionization and Photoelectron Spectroscopy* (Academic, New York, 1979), p. 80.
[89] E. Eggarter, J. Chem. Phys. **62**, 833 (1975).
[90] W. F. Chan, G. Cooper, X. Guo, and C. E. Brion, Phys. Rev. A **45**, 1420 (1992).
[91] S. Daviel, C. E. Brion, and A. P. Hitchcock, Rev. Sci. Instrum. **55**, 182 (1984).
[92] W. L. Wiese, M. W. Smith, and B. M. Glenon, *Atomic Transition Probabilities: Hydrogen through Neon,* Natl. Stand. Ref. Data Ser., Natl. Bur. Stand. U.S.) Circ. No. 4 (U.S. GPO, Washington, D.C., 1966), Vol. I.
[93] R. P. Madden, D. L. Ederer, and K. Codling, Phys. Rev. **177**, 136 (1969).
[94] B. L. Henke, P. Lee, T. J. Tanaka, R. L. Shimabukuro, and B. K. Fujikawa, At. Data Nucl. Data Tables **27**, 1 (1982).
[95] C. E. Moore, *Atomic Energy Levels,* Natl. Bur. Stand. (U.S.) Circ. No. 467 (U.S. GPO, Washington, D.C., 1949), Vol. 1; (1952), Vol. 2; (1958), Vol. 3.
[96] C. E. Kuyatt, quoted in Ref. [89] as private communication.
[97] W. L. Wiese, M. W. Smith, and B. M. Miles, *Atomic Transition Probabilities: Sodium through Calcium,* Natl. Stand. Ref. Data Ser., Natl. Bur. Stand. (U.S.) Circ. No. 22 (U.S. GPO, Washington, D.C., 1969), Vol. II.
[98] J. A. R. Samson, Phys. Rev. **132**, 2122 (1963).
[99] K. Codling and R. P. Madden, Phys. Rev. A **4**, 2261 (1971).
[100] D. L. Ederer, Phys. Rev. A **4**, 2263 (1971).
[101] K. Codling and R. P. Madden, J. Res. Natl. Bur. Stand. Sec. A **76**, 1 (1972).
[102] A. A. Wills, A. A. Cafolla, F. J. Currell, J. Comer, A. Svensson, and M. A. MacDonald, J. Phys. B **22**, 3217 (1989).
[103] A. A. Wills, A. A. Cafolla, and J. Comer, J. Phys. B **23**, 2029 (1990).
[104] M. G. Flemming, J. Z. Wu, C. D. Caldwell, and M. O. Krause, Phys. Rev. A **44**, 1733 (1991).